Non-parametric wall model and methods of identifying boundary conditions for moments in gas flow equations

Meng Liao, Quy-Dong To, Céline Léonard, Vincent Monchiet

Non-parametric wall model and methods of identifying boundary conditions for moments in gas flow equations

Meng Liao, Quy-Dong To,* Céline Léonard, and Vincent Monchiet

Université Paris-Est, Laboratoire Modelisation et Simulation Multi Echelle, UMR 8208 CNRS, 5 Boulevard Descartes, 77454 Marne-la-Vallée Cedex 2, France

(Dated: March 2, 2018)

Abstract

In this paper, we use Molecular Dynamics (MD) simulation method to study gas-wall boundary conditions. Discrete scattering information of gas molecules at the wall surface are obtained from collision simulations. The collision data can be used to identify the accommodation coefficients for parametric wall models such as Maxwell, Cercignani-Lampis scattering kernels. Since these scattering kernels are based on a limited number of accommodation coefficients, we adopt non-parametric statistical methods to construct the kernel to overcome these issues. Different from parametric kernels, the non-parametric kernels require no parameter (i.e accommodation coefficients) and no predefined distribution. We also propose approaches to derive directly the Navier friction and Kapitza thermal resistance coefficients as well as other interface coefficients associated to moment equations from the non-parametric kernels. The methods are applied successfully to systems composed of CH_4 or CO_2 and graphite, which are of interest to the petroleum industry.

PACS numbers:

* Corresponding author: quy-dong.to@u-pem.fr

I. INTRODUCTION

The study of transport properties in porous media plays an important role in many applications such as soil mechanics, geohydrology and the storage of nuclear waste. Along with the development of unconventional reservoirs (shale gas) extraction technology, like hydraulic fracturing, more attention has been paid to the transport of gas molecules in carbon pores. As a result, modeling the gas behavior and its interaction with the boundary is of significant interest.

Due to the size of the pore, gaseous molecules, here methane (CH_4) and carbon dioxide (CO_2) in this study, can travel with few collisions, resulting in high Knudsen number (Kn), a similar situation as the rarefaction effect. It is known that when $\mathrm{Kn} > 0.01$, predictions based on the continuum Navier-Stokes-Fourier (NSF) equations and classical no-slip, no-jump conditions are no longer in agreement with experiences and atomistic simulation results [1, 2]. In order to capture these phenomena, more advanced continuum equations and boundary conditions are necessary [3, 4].

Unlike liquids where the friction and thermal resistance are characterized by layers of interacting molecules adsorbed at the wall [5–7], the gas molecules collide infrequently and their residence time near the wall can be neglected. The exchange of momentum and energy between the gas and the wall can be understood from ensemble of independent gas-wall collisions. In most cases, the collisions are usually modeled with scattering kernels based on several accommodation coefficients [8–14]. Other class of wall models for rough surfaces [15–17] were analytically derived from corrugation parameter and potential well depth. Although these parametric models are simple to code, they rely on many oversimplification hypotheses which cannot guarantee the accuracy of the collisions for the whole velocity range. These problems can have consequences on the boundary conditions at the continuum level and simulation results based on these scattering kernels.

The paper presents a systematic study of gas-wall collision models based on Molecular Dynamics (MD) simulations. The systems in consideration are composed of methane CH_4 (considered as monatomic gas) or carbon dioxide CO_2 (rigid linear molecule) interacting

with a graphite wall constituted of carbon atoms. By beaming independently gas molecules onto the surface and recording the reflected flux, we can determine the accommodation coefficients. More importantly, we can reconstruct numerically a non-parametric (NP) wall model. Different from parametric models in literature, this scattering kernel is able to capture the reflection process in a more realistic way. Originated from non-parametric statistics, the NP scattering kernel requires no parametrization (i.e accommodation coefficients) and no predefined analytical form. Interestingly, it can be used to directly determine the parameters of any phenomenological boundary conditions, including those for NSF or moment equations. While these equations are valid for a limited range of Kn in the transition regime, the NP wall model can be directly implemented in particle methods like DSMC (Direct Simulation Monte Carlo) or MD to simulate flows at any Kn number. The development of gas-wall boundary conditions for continuum equations from a non-parametric kernel is the major contribution of the present work, which will be detailed in the subsequent sections.

II. STUDY OF GAS-WALL MODELS WITH MOLECULAR DYNAMICS METHOD

A. Scattering kernels

In kinetic theory, the state of monatomic gas at any location $\boldsymbol{x}$ at time t is entirely determined from the local number density $n(\boldsymbol{x}, t)$ and the probability density function $f(\boldsymbol{x}, \boldsymbol{c}, t)$ of velocity $\boldsymbol{c}$. The evolution of the latter is governed by the Boltzmann equation and the boundary conditions

$$c_z(nf)^+(\boldsymbol{c}) = \int_{\Omega^-} B(\boldsymbol{c}|\boldsymbol{c}')|c'_z|(nf)^-(\boldsymbol{c}')d\boldsymbol{c}', \quad \boldsymbol{c}' \in \Omega^-, \quad \boldsymbol{c} \in \Omega^+. \tag{1}$$

In the above expression, we assume that the boundary is normal to the z direction, and time t and space $\boldsymbol{x}$ variables are dropped for simplicity. Eq. (1) connects the incoming flux $c'_z(nf)^-(\boldsymbol{c}')$ and the outgoing flux $c_z(nf)^+(\boldsymbol{c})$ via the scattering kernel $B(\boldsymbol{c}|\boldsymbol{c}')$. The two velocities $\boldsymbol{c}$ and $\boldsymbol{c}'$ belong to dual half-spaces Ω^- and Ω^+ in $\mathbb{R}^3$, respectively, defined below

$$\boldsymbol{c}' \in \Omega^- = \mathbb{R}^2 \times \mathbb{R}^-, \quad \boldsymbol{c} \in \Omega^+ = \mathbb{R}^2 \times \mathbb{R}^+. \tag{2}$$

For fluid in equilibrium, the distribution of velocity is equal to the Maxwell-Boltzmann distribution

$$f_{eq}(\boldsymbol{c}) = f_M(\boldsymbol{c}) = \frac{1}{\sqrt{2\pi\theta}^3} \exp\left[-\frac{\boldsymbol{c}^2}{2\theta}\right], \quad \theta = k_B T/m, \tag{3}$$

where k_B is the Boltzmann constant, m the atomic mass, and T the temperature. For rigid gas molecules, in addition to translational velocity of the center of mass, we must account for the rotational velocity $\boldsymbol{\omega}$. The scattering kernel must be replaced by $B(\boldsymbol{\omega}, \boldsymbol{c}|\boldsymbol{\omega}', \boldsymbol{c}')$ and the probability density by $f(\boldsymbol{\omega}, \boldsymbol{c})$. The two half-spaces Ω^- and Ω^+ are also extended to include the rotational velocity $\boldsymbol{\omega}$, e.g $\Omega^- = \mathbb{R}^5 \times \mathbb{R}^-$ for incident molecules and $\Omega^+ = \mathbb{R}^5 \times \mathbb{R}^+$ for reflected molecules. It is possible to include the orientation distribution in the scattering kernel but this will not be considered in the present work. At equilibrium, this density function is given by

$$f_{eq}(\boldsymbol{\omega}, \boldsymbol{c}) = f_M(\boldsymbol{c}) f_M^{\omega}(\boldsymbol{\omega}), \quad f_M^{\omega}(\boldsymbol{\omega}) = \frac{1}{\sqrt{2\pi\theta^{\omega}}^d} \exp\left[-\frac{\boldsymbol{\omega}^2}{2\theta^{\omega}}\right], \quad \theta^{\omega} = k_B T/I. \tag{4}$$

The quantity I represents the moment of inertia and the power d the rotational degree of freedom, $d = 2$ for linear molecules and $d = 3$ otherwise. It is noted that for linear molecules, the rotation around its proper axis is not considered.

The scattering kernel $B(\boldsymbol{\omega}, \boldsymbol{c}|\boldsymbol{\omega}', \boldsymbol{c}')$ which is the probability of finding molecules bouncing with velocity $(\boldsymbol{\omega}, \boldsymbol{c})$ with given colliding velocities $(\boldsymbol{\omega}', \boldsymbol{c}')$ can be determined by Molecular Dynamics collision simulation. Gas molecules are beamed at given velocities $(\boldsymbol{\omega}', \boldsymbol{c}')$ onto the surface in consideration and the velocity distribution of reflecting molecules associated to $(\boldsymbol{\omega}', \boldsymbol{c}')$ is recorded. Next the arriving velocities $(\boldsymbol{\omega}', \boldsymbol{c}')$ are also varied to cover the incident velocity space. Generally, if the number of realizations is sufficiently large, we have a large set of discrete points which can represent the true probability density $B(\boldsymbol{\omega}, \boldsymbol{c}|\boldsymbol{\omega}', \boldsymbol{c}')$.

We are also concerned about the use of the kernel as wall boundary conditions in other simulation methods (for example Molecular Dynamics, Direct Simulation Monte Carlo or Lattice Boltzmann). If we use the discrete form of $B(\boldsymbol{\omega}, \boldsymbol{c}|\boldsymbol{\omega}', \boldsymbol{c}')$, output results must be obtained from the interpolation of known points. This method is accurate but less computationally convenient. The scattering kernel can be analytically modeled using some physical

This manuscript was accepted by Phys. Fluids. Click here to see the version of record.

parameters for example Tangential Momentum Accommodation Coefficients (TMAC) or Energy Momentum Accommodation Coefficients (EAC), etc... Some notable scattering models are Maxwell-Yamamoto (MY) [11], Cercignani-Lampis (CL) [9] etc... which can be used for atomistic gas flow simulations and accommodation coefficients can be used to derive velocity slip and temperature jump coefficients for NSF equations. To account for the special reflection mechanism of the anisotropic surface, one can use Dadzie-Meolans (DM) kernel [18] or anisotropic Cercignani-Lampis (ACL) kernel [14] with three different coefficients associated to the three directions x, y, z.

The MD collision point cloud can be fitted by analytical scattering models and the model parameters can be identified. However, the data can be scattered and there is no truly efficient fitting algorithm, for example, one can use the mean square of the difference between the two probability densities or methods based on accommodation parameters. We note that constant accommodation coefficients are only meaningful for analytical scattering kernel listed previously. For realistic gas surface interaction, those coefficients are usable in approximative sense and can oversimplify the true behavior.

B. Expressions for fluxes, average values and accommodation coefficients

Given molecular quantities Q as function of velocities $\boldsymbol{c}, \boldsymbol{\omega}$, the average value $\overline{Q}$ and the flux Φ_Q across a plane normal to z can be computed as

$$\overline{Q} = \int Q(\boldsymbol{c}, \boldsymbol{\omega}) f d\boldsymbol{c} d\boldsymbol{\omega}, \quad \Phi_Q = n \int Q(\boldsymbol{c}, \boldsymbol{\omega}) c_z f d\boldsymbol{c} d\boldsymbol{\omega}. \tag{5}$$

Given the fact that all the physical quantities such as density n, temperature T, stress $\boldsymbol{\sigma}$, velocity v, and heat flux $\boldsymbol{q}$ are either average value or flux of molecular quantities, it is possible to investigate their relations at the boundary by examining the gas wall collisions. With respect to the wall normal to the z direction, we define influx Φ_Q^- and outflux Φ_Q^+ of atomic quantity $Q(\boldsymbol{c}, \boldsymbol{\omega})$ at the wall via the expressions

$$\Phi_Q^- = \int_{\Omega^-} |c_z| (nf)^- Q(\boldsymbol{c}, \boldsymbol{\omega}) d\boldsymbol{c} d\boldsymbol{\omega}, \quad \Phi_Q^+ = \int_{\Omega^+} |c_z| (nf)^+ Q(\boldsymbol{c}, \boldsymbol{\omega}) d\boldsymbol{c} d\boldsymbol{\omega}. \tag{6}$$

This manuscript was accepted by Phys. Fluids. Click here to see the version of record.

From atomistic viewpoint, Φ_Q^-, Φ_Q^+ can be computed by counting the number of atoms N crossing the control plane in a given time t

$$\Phi_Q^- = \frac{1}{t}\sum_{incident} Q(\boldsymbol{c},\boldsymbol{\omega}) = \frac{N}{t}\langle Q\rangle_i = \nu\langle Q\rangle_i, \quad \Phi_Q^+ = \nu\langle Q\rangle_o, \tag{7}$$

where the subscript i stands for input (incident), o for output (reflection), ν collision rate. Here the notation $\langle Q\rangle$ is the average of molecular quantities Q that cross the control plane in Molecular Dynamics simulations. By breaking each relation in (5) into two integrals in half-spaces Ω^- and Ω^+ as follows

$$\begin{aligned} n\overline{Q} &= \int_{\Omega^-} \frac{Q(\boldsymbol{c},\boldsymbol{\omega})}{|c_z|}|c_z|(nf)^- d\boldsymbol{c}d\boldsymbol{\omega} + \int_{\Omega^+} \frac{Q(\boldsymbol{c},\boldsymbol{\omega})}{|c_z|}|c_z|(nf)^+ d\boldsymbol{c}d\boldsymbol{\omega}, \\ \Phi_Q &= -\int_{\Omega^-} Q(\boldsymbol{c},\boldsymbol{\omega})|c_z|(nf)^- d\boldsymbol{c}d\boldsymbol{\omega} + \int_{\Omega^+} Q(\boldsymbol{c},\boldsymbol{\omega})|c_z|(nf)^+ d\boldsymbol{c}d\boldsymbol{\omega}, \end{aligned} \tag{8}$$

and making use of (7) and (6), the flux Φ_Q and the average value $\overline{Q}$ at the wall can also be expressed as

$$n\overline{Q} = \Phi^+_{Q/|c_z|} + \Phi^-_{Q/|c_z|} = \nu\langle Q/|c_z|\rangle_{i+o}, \quad \Phi_Q = \Phi_Q^+ - \Phi_Q^- = \nu\langle Q\rangle_{o-i}, \tag{9}$$

with notation $\langle Q\rangle_{\alpha\pm\beta} := \langle Q\rangle_\alpha \pm \langle Q\rangle_\beta$. The relation between the average value $\overline{Q}$, and fluxes $\Phi^+_{Q/|c_z|}$ and $\Phi^-_{Q/|c_z|}$ is useful because it is more convenient to compute $\overline{Q}$ with MD simulations. Choosing $Q = 1$ in (9) and noting that $\overline{Q} = \langle Q\rangle_i = \langle Q\rangle_o = 1$, we have the equalities

$$\nu = n\frac{1}{\langle 1/|c_z|\rangle_{i+o}}, \quad \Phi_1 = 0. \tag{10}$$

Substituting ν/n from the first expression in (10) back into (9) for the general Q, we can derive that

$$\overline{Q} = \frac{\langle Q/|c_z|\rangle_{i+o}}{\langle 1/|c_z|\rangle_{i+o}}, \quad \Phi_Q = \frac{n\langle Q\rangle_{o-i}}{\langle 1/|c_z|\rangle_{i+o}}. \tag{11}$$

We remark that the second relation of (10) is equivalent to the no atom accumulation condition at the wall, i.e the influx is equal to the outflux. If the leaving atoms are fully thermalized by the wall, the phase density f^+ should be replaced by the equilibrium distribution $f_{eq}(\boldsymbol{\omega},\boldsymbol{c})$ at the wall temperature T_w. The outgoing flux $\Phi^+_{Q_w}$ associated to this

This manuscript was accepted by Phys. Fluids. Click here to see the version of record.

distribution is given by the expression

$$\Phi^+_{Q_w} = \int_{\Omega^+} |c_z| n f_{eq}(\boldsymbol{\omega}, \boldsymbol{c}) Q d\boldsymbol{c} d\boldsymbol{\omega} = \nu \langle Q \rangle_w, \tag{12}$$

where the subscript w is for outgoing flux at the wall temperature T_w. Since $f_{eq}(\boldsymbol{\omega}, \boldsymbol{c})$ is known from (4) and ν is estimated by setting $Q = 1$, we can compute the expected values for thermal wall $\langle Q \rangle_w$. They are functions of the reduced wall temperature $\theta_w = k_B T_w / m$ and given in Tab I. It is noted that for the special case where $d = 0$, the tabulated values are consistent with previous works for monatomic gas [19].

Component	Velocity	Energy
Tangential (x, y)	$\langle c_x \rangle_w = 0$	$\langle c_x^2 \rangle_w = \theta_w$
Normal (z)	$\langle c_z \rangle_w = \frac{1}{2}\sqrt{2\pi\theta_w}$	$\langle c_z^2 \rangle_w = 2\theta_w$
Total	$\langle c \rangle_w = \frac{3}{4}\sqrt{2\pi\theta_w}$	$\langle c^2 + \frac{I}{m}\omega^2 \rangle_w = (4+d)\theta_w$

TABLE I. Expected values as functions of the reduced wall temperature $\theta_w = k_B T_w / m$. For CH_4, the rotation energy is neglected $d = 0$ and for CO_2, $d = 2$.

As a result, the accommodation coefficient of quantity Q is equivalent to the expression

$$\alpha_Q = \frac{\Phi^-_Q - \Phi^+_Q}{\Phi^-_Q - \Phi^+_{Q_w}} = \frac{\langle Q \rangle_{i-o}}{\langle Q \rangle_{i-w}} \quad \text{or} \quad \langle Q \rangle_o = (1 - \alpha_Q)\langle Q \rangle_i + \alpha_Q \langle Q \rangle_w. \tag{13}$$

The above expression which is independent of the collision rate ν, is useful for the determination of the accommodation coefficients using MD method. Usually, the value for $\langle Q \rangle_w$ is known explicitly (see Tab I) and the coefficient can be computed based on Eq. (13). Most analytical wall models in literature are based on constant accommodation coefficients, which are independent of the input data nf^-. These assumptions may not be true for a general kernel $B(\boldsymbol{\omega}, \boldsymbol{c} | \boldsymbol{\omega}', \boldsymbol{c}')$ and this is the major disadvantage of using accommodation coefficients to model realistic surfaces.

When accommodation coefficients are not properly defined, different methods can be used to compute those coefficients and result differently. For example, in Ref.[19], the authors

proposed using the least-squares formula

$$\alpha_Q = 1 - \frac{\sum_{collision}(Q_i - \langle Q\rangle_i)(Q_o - \langle Q\rangle_o)}{\sum_{collision}(Q_i - \langle Q\rangle_i)^2}, \tag{14}$$

from the collision clouds. They found that results are very different from those obtained by Eq. (13).

These observations pose some problems on theories based on the existence of the constant accommodation coefficients for general surfaces. However, interface phenomena like slip velocity and temperature jumps do exist. Modeling those effects and identifying the parameters without using accommodation coefficients will be considered in the following.

C. Boundary conditions for Navier Stokes Fourier (NSF) equations

In this subsection, we present a new method to directly determine the macroscopic velocity and temperature jump coefficients via collision simulations. This completely avoids the intermediate modeling and simulations based on scattering kernels. As we know, all available analytical models have limitations. First, they only allow at most three accommodation coefficients. If we choose to model momentum accommodation effect along one direction, we have to sacrifice the energy accommodation along this direction. Accommodation effects for high order moment are also unavailable. Secondly, using constant accommodation coefficients, like most analytical wall models in literature can be a strong assumption. Numerical evidence in the latter section shows that in some cases, the true behavior deviates significantly from that hypothesis.

The approach proposed here is independent of scattering model and can be applied to any surfaces. It can also be extended to deal with general boundary conditions involving higher order moments. In slip regimes, the usual macroscopic boundary conditions for velocities v_x, v_y and reduced temperature jump $\theta - \theta_w$ are given in the following forms

$$v_k = -\frac{2-\alpha_k}{\alpha_k}\frac{\sigma_{kz}}{nm\sqrt{2\theta/\pi}}, \quad \theta - \theta_w = -\frac{2-\alpha_e}{2\alpha_e}\frac{q_z}{nm\sqrt{2\theta/\pi}}, \quad k = x, y, \tag{15}$$

This manuscript was accepted by Phys. Fluids. Click here to see the version of record.

where σ_{xz}, σ_{yz} are the (minus) shear stress components and q_z the normal heat flux at the wall. Constants α_k are the tangential accommodation coefficients associated to the tangential translational molecular velocities, and α_e is the energy accommodation coefficient associated to its kinetic energy. The above equation where the thermal transpiration is neglected can be derived from the scattering models. In this paper, we propose a more general phenomenological form for the boundary conditions

$$\beta_{1k} v_k = -\frac{\sigma_{kz}}{nm\sqrt{2\theta/\pi}}, \quad \beta_2(\theta - \theta_w) = -\frac{q_z}{2nm\sqrt{2\theta/\pi}}, \quad k = x, y, \tag{16}$$

where β_{1x}, β_{1y} and β_2 are the dimensionless friction and Kapitza coefficients, depending on the gas-wall couple. It is clear that we recover the original equation if the coefficients β_{1k} and β_2 are connected to the accommodation coefficients α_k and α_e via the relation

$$\beta_{1k} = \frac{\alpha_k}{2 - \alpha_k}, \quad \beta_2 = \frac{\alpha_e}{2 - \alpha_e}, \quad k = x, y, \tag{17}$$

It is noted that the two expressions in (16) can also be used for the cases where the accommodation coefficients are not constant.

Using Eqs. (7-11), we shall derive schemes to determine β_{1k} and β_2 from MD simulations. The velocity defined as $v_k = \overline{c_k}$ (i.e $Q = c_k$) can be computed by the expression

$$v_k = \frac{\langle c_k/|c_z|\rangle_{i+o}}{\langle 1/|c_z|\rangle_{i+o}}. \tag{18}$$

The (minus) shear stress $\sigma_{kz} = \Phi_{mC_k}$ (i.e $Q = mC_k$) can also be computed in the following way

$$-\sigma_{kz} = m\nu(\langle C_k\rangle_i - \langle C_k\rangle_o) = mn\frac{\langle c_k\rangle_i - \langle c_k\rangle_o}{\langle 1/|c_z|\rangle_i + \langle 1/|c_z|\rangle_o} = mn\frac{\langle c_k\rangle_{i-o}}{\langle 1/|c_z|\rangle_{i+o}}, \tag{19}$$

where $C_k = c_k - v_k$ is the peculiar velocity. Comparing Eqs. (18,19) with (16), we can derive the interface coefficients β_{ik} via the expression

$$\beta_{1k} = \frac{\langle c_k\rangle_{i-o}/\sqrt{2\theta/\pi}}{\langle c_k/|c_z|\rangle_{i+o}}. \tag{20}$$

This manuscript was accepted by Phys. Fluids. Click here to see the version of record.

Next, the reduced temperature $\theta = \overline{C^2 + (I/m)\omega^2}/(3+d)$ and the heat flux $q_z = \Phi_{(mC^2+I\omega^2)/2}$ are given by the equation

$$\theta = \frac{\langle (C^2 + (I/m)\omega^2)/|c_z|\rangle_{i+o}}{(3+d)\langle 1/|c_z|\rangle_{i+o}}, \quad -q_z = mn\frac{\langle (C^2 + (I/m)\omega^2)/2\rangle_{i-o}}{\langle 1/|c_z|\rangle_{i+o}}, \tag{21}$$

where d is the number of rotation degrees of freedom of gas molecule, $d = 2$ for CO_2. Comparing Eqs. (21) with (16), we can calculate the Kapitza coefficient

$$\beta_2 = \frac{(3+d)\langle (C^2 + (I/m)\omega^2)/2\rangle_{i-o}/(4\theta/\pi)}{[\langle (C^2 + (I/m)\omega^2)/|c_z|\rangle_{i+o} - (3+d)\theta_w\langle 1/|c_z|\rangle_{i+o}]/\sqrt{2\theta/\pi}}. \tag{22}$$

We note that for monatomic gas, it is sufficient to remove the terms $I\omega^2$ and d in the above expression and obtain

$$\beta_2 = \frac{3\langle C^2/2\rangle_{i-o}/(4\theta/\pi)}{[\langle C^2/|c_z|\rangle_{i+o} - 3\theta_w\langle 1/|c_z|\rangle_{i+o}]/\sqrt{2\theta/\pi}}. \tag{23}$$

To facilitate the comparison between the numerical results, we normalize stress and heat flux computed by MD method with suitable quantities and rewrite the phenomenological law in the following way

$$\beta_{1k} = \frac{-\hat{\sigma}_{kz}}{\hat{v}_k}, \quad \beta_2 = \frac{-\hat{q}_z}{\Delta\hat{\theta}}, \quad k = x, y. \tag{24}$$

Here, the hat notation is used for the normalized quantities,

$$\hat{\sigma}_{kz} = \frac{\sigma_{kz}}{nm\zeta^2}, \quad \hat{v}_k = \frac{v_k}{\zeta}, \quad \hat{q}_z = \frac{q_z}{2nm\zeta^3}, \quad \Delta\hat{\theta} = \frac{\theta - \theta_w}{\zeta^2}, \quad \zeta = \sqrt{2\theta/\pi}. \tag{25}$$

D. Extension to 13 moments equations

Without being limited to NSF equations, the method presented previously can be applied to higher order model. Given any macroscopic boundary conditions in terms of moments, the present method can be used to derive the coefficients associated to boundary conditions. As an example, we consider the boundary conditions of R13 equations written for isotropic surfaces in dimensionless form[3, 20]

$$\beta_1 = \frac{-\hat{\sigma}_{xz}}{\hat{\kappa}_1}, \quad \beta_2 = \frac{-\hat{q}_z}{\hat{\kappa}_2}, \quad \beta_3 = \frac{-\hat{m}_{xxz}}{\hat{\kappa}_3}, \quad \beta_4 = \frac{\hat{m}_{zzz}}{\hat{\kappa}_4}, \quad \beta_5 = \frac{\hat{R}_{xz}}{\hat{\kappa}_5}, \tag{26}$$

with

$$\hat{m}_{ijl} = \frac{m_{ijl}}{nm\zeta^3}, \quad \hat{R}_{ij} = \frac{R_{ij}}{nm\zeta^2},$$
$$\hat{\kappa}_1 = \sqrt{\frac{2}{\pi\theta}}\left(Pv_x + \frac{1}{2}m_{xzz} + \frac{1}{5}q_x\right)/(nm\zeta^2),$$
$$\hat{\kappa}_2 = \sqrt{\frac{2}{\pi\theta}}\left(2P(\theta-\theta_w) - \frac{1}{2}Pv^2 + \frac{1}{2}\theta\sigma_{zz} + \frac{R}{15} + \frac{5}{28}R_{zz}\right)/(2nm\zeta^3),$$
$$\hat{\kappa}_3 = \sqrt{\frac{2}{\pi\theta}}\left(\frac{1}{14}R_{xx} + \theta\sigma_{xx} - \frac{1}{5}\theta\sigma_{zz} + \frac{1}{5}P(\theta-\theta_w) - \frac{4}{5}Pv_x^2 - \frac{R}{150}\right)/(nm\zeta^3),$$
$$\hat{\kappa}_4 = \sqrt{\frac{2}{\pi\theta}}\left(\frac{2}{5}P(\theta-\theta_w) - \frac{1}{14}R_{zz} - \frac{3}{5}Pv^2 - \frac{7}{5}\theta\sigma_{zz} + \frac{R}{75}\right)/(nm\zeta^3),$$
$$\hat{\kappa}_5 = \sqrt{\frac{2}{\pi\theta}}\left(P\theta v_x - \frac{11}{5}\theta q_x - \frac{1}{2}\theta m_{xzz} - Pv^2v_x + 6Pv_x(\theta-\theta_w)\right)/(nm\zeta^4). \tag{27}$$

The quantities P, R, R_{ij} and m_{ijl} are defined from the moments

$$P = nm\theta + \frac{1}{2}\sigma_{zz} - \frac{1}{120}\frac{R}{\theta} - \frac{1}{28}\frac{R_{zz}}{\theta}, \quad R_{ij} = mn\overline{C^2(C_iC_j - C^2/3\delta_{ij})} - 7\theta\sigma_{ij},$$
$$R = mn(\overline{C^4} - 15\theta^2), \quad m_{ijl} = mn\overline{C_iC_jC_l - C^2(C_i\delta_{jl} + C_j\delta_{il} + C_l\delta_{ij})/5},$$
$$k = x, y, \quad i, j, l = x, y, z. \tag{28}$$

These original boundary conditions are derived for Maxwell molecules and Maxwell scattering kernel where all the coefficients are identical $\beta_1 = \beta_2 = ... = \beta_5 = \alpha/(2-\alpha)$ with α being the accommodation coefficient. Moments R, R_{ij} and m_{ijl} are connected to stress, heat flux, velocity, temperature and their derivatives via a regularization procedure [3, 21, 22].

Although the derivation conditions are rather restrictive, we shall assume that they are valid and determine the coefficients $\beta_1, \beta_2, ..., \beta_5$. We shall base directly on the moment definitions Eqs. (28) which are independent of the regularization methods and also relax the conditions that all coefficients $\beta_1, \beta_2, ..., \beta_5$ must be identical. We note that in Ref. [21], these authors already consider that $\beta_1, \beta_2, ..., \beta_5$ can be different and take empirical values allowing matching with a more accurate method. In these cases, those coefficients are used to fix the Knudsen layer effect that the R13 equation fails to capture completely. This empirical approach seems to be incompatible with the rigorous mathematical derivation of R13 equations.

This manuscript was accepted by Phys. Fluids. Click here to see the version of record.

E. Generation of pre-collision velocity

Molecular Dynamics simulation requires generating velocities of atoms that cross the control plane and collide with the wall. The (unnormalized) distribution of the latter is $|c_z|f^-(\boldsymbol{c},\boldsymbol{\omega})$ with $c_z < 0$ as seen in the previous section. In this paper, we use three types of distribution

- The Maxwell Boltzmann (MB) distribution

$$\begin{aligned} &\text{For molecular gas } |C_z|f^-(\boldsymbol{c},\boldsymbol{\omega}) = |C_z|f_M(\boldsymbol{C})f_M^{\omega}(\boldsymbol{\omega}).\\ &\text{For monatomic gas } |c_z|f^-(\boldsymbol{c}) = |c_z|f_M(\boldsymbol{C}). \end{aligned} \tag{29}$$

The parameters of the distribution are the mean velocity $\boldsymbol{v}$ and the reduced temperature θ. Using this distribution, we can model equilibrium system where the fluid is stationary $\boldsymbol{v} = 0$ and the temperature is uniform $\theta = \theta_w$ or non-equilibrium system by assuming that the gas adjacent to the wall is in local equilibrium with temperature and velocity different from the wall, i.e $\boldsymbol{v} \neq 0$, $\theta \neq \theta_w$.

- The Chapman-Enskog (CE) distribution [23, 24]

$$|c_z|f^-(\boldsymbol{c}) = |C_z|f_{CE}(\boldsymbol{C}). \tag{30}$$

In addition to temperature θ and mean velocity $\boldsymbol{v}$, there are also parameters associated to heat flux q_k and shear stress σ_{ik}. This distribution is for non-equilibrium monatomic gas.

- The R13 distribution [20, 22]

$$|c_z|f^-(\boldsymbol{c}) = |C_z|f_{R13}(\boldsymbol{C}). \tag{31}$$

The last two distributions CE and R13 are for monatomic gases with expressions given in Appendix A. The generation of the input velocity is done via the Acceptance-Rejection approach. For example, in Ref. [25], a scheme to generate distributions in the form $f(\boldsymbol{c}) = f_M(\boldsymbol{C})\Gamma(\boldsymbol{C})$ where $\Gamma(\boldsymbol{C})$ is a polynomial of $\boldsymbol{C}$, is proposed. The distribution to be treated in this paper is slightly different since we are limited to the half-space $c_z < 0$ and there is a

function $|c_z|$ standing before $f_M(\boldsymbol{C})$ due to the flux definition (see Appendix A).

III. NUMERICAL SIMULATIONS AND RESULTS

A. Molecular Dynamics model

We study the collision of gas molecules, methane (CH_4) and carbon dioxide (CO_2) on a graphite wall (C atoms). The system contains two parts: the reservoir and the collision zone. The MD simulation is only done in the collision zone and the pre-collision velocity of gas molecules is generated directly at the stochastic boundary between the reservoir and the collision zone. Two graphite wall models will be considered. The first is a smooth wall model composed of 3 graphene layers with dimensions 17.04 Å × 17.22 Å (336 carbon atoms). The second is a rough model where a narrower band of graphene with surface 8.52 Å × 17.22 Å is added on the smooth surface (392 carbon atoms). Due to the surface geometry and symmetry, the scattering behavior of the smooth model is close to being isotropic and that of the rough model is anisotropic. We define the x and y directions as respectively "armchair" and "zigzag" directions, and the z direction as the normal direction to the graphite plane. During the simulation, the lowest sheet is fixed and the second layer is maintained at constant temperature (350 K for CH_4 model and 600 K for CO_2 model) by Nose-Hoover thermostat with the relaxing temperature parameter equals to 100 time steps. The two final layers are free to interact with the gas molecules. We use periodic boundary conditions for x, y directions, and we fix the height of box along z direction. The gas-wall truncation distance is set to 15 Å from the upper layer, and the stochastic boundary is located at the truncation distance from the graphite wall. A simple sketch of the system and snapshots of MD simulations are shown in Fig. 1.

All MD simulations are performed with LAMMPS (Large-scale Atomic/Molecular Massively Parallel Simulator) package [26]. A typical simulation of 10^5 collisions takes roughly 50 hours on an architecture of 92 Intel(R) Xeon(R) processors 2-3 GHz. The adaptive intermolecular reactive bond order (AIREBO) potential [27] is used for the interaction between the graphite carbon atoms. The CH_4 molecule is modeled as a united atom and its

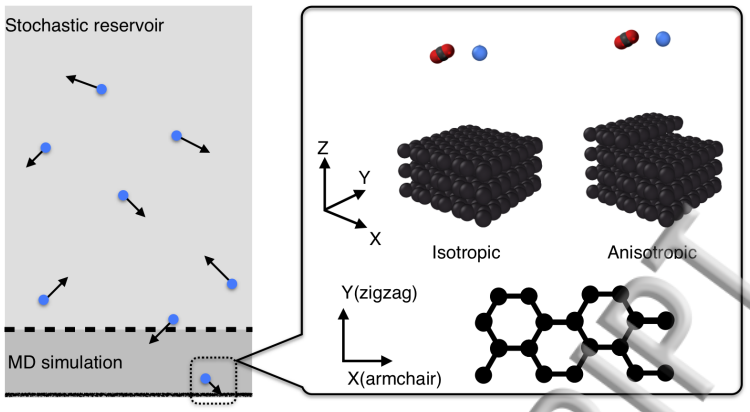

FIG. 1. Simple sketch of the system. The stochastic boundary is indicated by the dashed line and the graphite wall is indicated by the solid line. Snapshots of MD simulations show the local orientation of the smooth (isotropic) and rough (anisotropic) systems.

interaction with graphite atoms is governed by the Lennard Jones (LJ) potential

$$V = 4\epsilon\left[\left(\frac{\sigma}{r}\right)^{12} - \left(\frac{\sigma}{r}\right)^{6}\right], \tag{32}$$

where r is the distance between two atoms under consideration and σ and ϵ the parameters of the LJ model. Regarding the CO_2 molecules, we do not consider the contribution of the internal degrees of freedom (bending/stretching) and use the rigid model [28]. The interaction of each site with the graphite atoms is also of LJ type with parameters taken from Ref. [5] (see Table II). After equilibrating the graphite system at the given temperature (10^6 time steps of 1 fs), gas molecules are inserted one by one in the collision zone. Only after one collision event, i.e a molecule interacts with the wall and goes out of the collision zone, another molecule is inserted in the zone from a random position at the stochastic boundary (for CH_4 and CO_2) and with a random orientation (for CO_2). The residence time is considered negligibly small with respect to the flying time outside this zone and the velocities at the entrance and the outlet are collected (see Fig. 2).

Some comments can be made about the models for CH_4 and CO_2 used in the present work. Both rigid molecule models do not account for the vibrational internal degrees of freedom. The bending mode of CO_2 associated with a wavenumber of 667 cm^{-1} [29] is the most concerned by an excitation due to collisions with the solid surface since this mode is the lowest energetic. The CO_2 molecule collides with a surface at 600 K, i.e. $k_BT = 417$

This manuscript was accepted by Phys. Fluids. Click here to see the version of record.

cm^{-1}. Using Boltzmann statistics, it can be estimated that only 20% of the CO_2 molecules may be concerned by such an excitation. The lowest energetic vibrational mode of CH_4 is the angle deformation mode associated with a wavenumber at 1306 cm^{-1} [29] and this molecule collides a surface at 350 K ($k_BT = 243$ cm^{-1}). The Boltzmann statistics indicate that only 5% of the molecules would be excited. From these estimates and for simplification, CO_2 and CH_4 are kept rigid.

	σ[Å]	ϵ[meV]
CH_4 - C (Graphite)	3.550	5.547
C (CO_2) - C (Graphite)	3.059	2.418
O (CO_2) - C (Graphite)	3.197	4.091

TABLE II. LJ parameters for the interaction of CH_4 and CO_2 with the graphite surface.

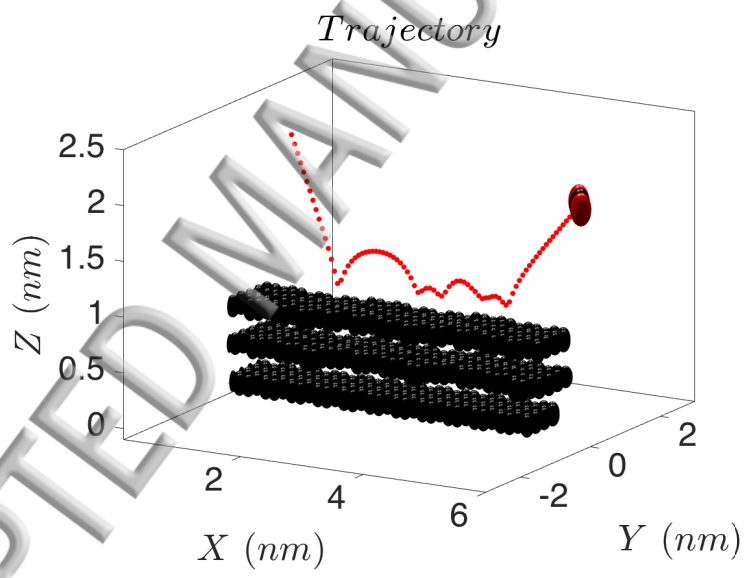

FIG. 2. A collision showing the trajectory of a gas molecule.

We implement 3 simulation schemes to study gas-wall models and determine the model coefficients. They are different in terms of the gas state (equilibrium/non-equilibrium) and the associated velocity generator.

- **Batch average (BA) scheme**: We repeat the same incident velocity $(\boldsymbol{\omega}', \boldsymbol{c}')$ many times and record the reflected velocity $(\boldsymbol{\omega}, \boldsymbol{c})$ which is a distribution. To generate samples, the incident velocity is taken from equilibrium distribution and the reflected velocity is aver-

aged. By this way [30], we can examine the accommodation coefficients via their definition (Eq. (13)). In Fig. 3, We have plotted the input quantities $\langle Q\rangle_i$ against output quantities $\langle Q\rangle_o$, where $Q = c_x, c_y, c_z$ or $c^2 + I\omega^2/m$. In the ideal case, the data population should concentrate along a straight line and its slope corresponds to the constant accommodation coefficient α_Q (see section III.B for details).

- **Stochastic equilibrium (SE) scheme**: The reservoir is considered to be in equilibrium. The pre-collision velocity $(\boldsymbol{\omega}', \boldsymbol{c}')$ for each collision is generated using equilibrium distribution at zero mean velocity and at the same temperature as the graphite wall. By this way, we obtain numerical estimates of the density $B(\boldsymbol{\omega}, \boldsymbol{c}|\boldsymbol{\omega}', \boldsymbol{c}')$. The accommodation coefficients can be extracted using (14) (see section III.B for details).

- **Stochastic non-equilibrium (SN) scheme**: The non-equilibrium gas is considered. Depending on the problems, we use Maxwell-Boltzmann (MB), Chapman Enskog (CE) or R13 distribution as discussed in the previous section. The surface can be modeled atomistically (AM) as described from the beginning of the present section III.A. It can also be modeled statistically using the non-parametric (NP) model $B(\boldsymbol{\omega}, \boldsymbol{c}|\boldsymbol{\omega}', \boldsymbol{c}')$. The latter is constructed by the scattering results on the atomic model, which is detailed at the end of section III.B.

The simulation results will be analyzed using the theory we have proposed in the previous section.

B. Determination of accommodation coefficients and construction of non-parametric wall model from collision data

As mentioned previously, the accommodation coefficients are parameters based on Eq. (13). To verify this assumption, it is sufficient to study incident fluxes of constant velocity. Using BA scheme for the couples CH_4/CO_2-Graphite (smooth and rough surfaces), we set up 100 sampling groups and each group contains 500 collisions with the same incident velocity. These 100 incident velocities are drawn from equilibrium distribution at the same temperature as the wall. Then, we average the reflected values in the group for later anal-

ings. Theoretically, if the ratio between the input and the output values are constant, the collision data will form a straight line. In Fig. 3, we find a strong correlation between the input and the output velocities. For the tangential velocity, despite some slight curvature the relation between the input and output is visibly linear for most of the data. However, the linear regression works less well for the normal velocity and especially for the kinetic energy. These data suggest that Eq. (13) is not valid for these cases and linear coefficients obtained by fitting (see Tab. III) are not representative.

Parametric studies based on varying the number of samples per input velocity from 20 to 1000 show that the scattering of energy data is always present. Given the fact that the results for c_x and c_y are clearly correlated, the energy data merit more detailed investigation to understand the origin of the deviation. We still use the same data and decompose the kinetic energy into tangential and normal components c_n^2, c_t^2. In Fig. 4(a) and (b), we can see that the tangential and normal kinetic energy data $\langle c_t'^2 \rangle$ vs. $\langle c_t^2 \rangle$, $\langle c_n'^2 \rangle$ vs. $\langle c_n^2 \rangle$ are strongly correlated. However, like the data $\langle c_x' \rangle$ vs. $\langle c_x \rangle$ and $\langle c_z' \rangle$ vs. $\langle c_z \rangle$ in Fig. 3, their slopes are different. There is a strong contrast between the tangential reflection c_t^2 which is more specular-like (energy mostly conserved after collision) and the normal reflection c_n^2 which is more diffusive-like (energy close to the walls' after collision). On the other hand, in Fig. 4(c) and (d), the data $\langle c_t'^2 \rangle$ vs. $\langle c_n^2 \rangle$ and $\langle c_n'^2 \rangle$ vs. $\langle c_t^2 \rangle$ are scattered and the correlation is weak. It is suggested that the combination of different tangential and normal reflection behaviors can be responsible for the scattering of the total energy data c^2. As a final remark, the energy data scattering exists in literature models, especially for parametric models like ACL/CL or DM which are not based on a constant energy accommodation coefficient. Indeed, Fig 5 shows that the parametric kernel ACL/CL with suitable parameters has produced the same pattern, i.e energy data scattering, as the MD results.

Next, with the SE scheme, we simulated 10^5 collisions on graphite surfaces. The input velocities are taken from equilibrium distribution and results are presented in Fig. 6. From these figures we can analyze the correlation between incident and reflected velocities on graphite wall then we can compute the accommodation coefficients from Eq. (14) issued from [19]. It is noted that due to the equilibrium state, Eq. (13) takes the form 0/0 and cannot be used to determine the accommodation coefficients in this case. We find that for

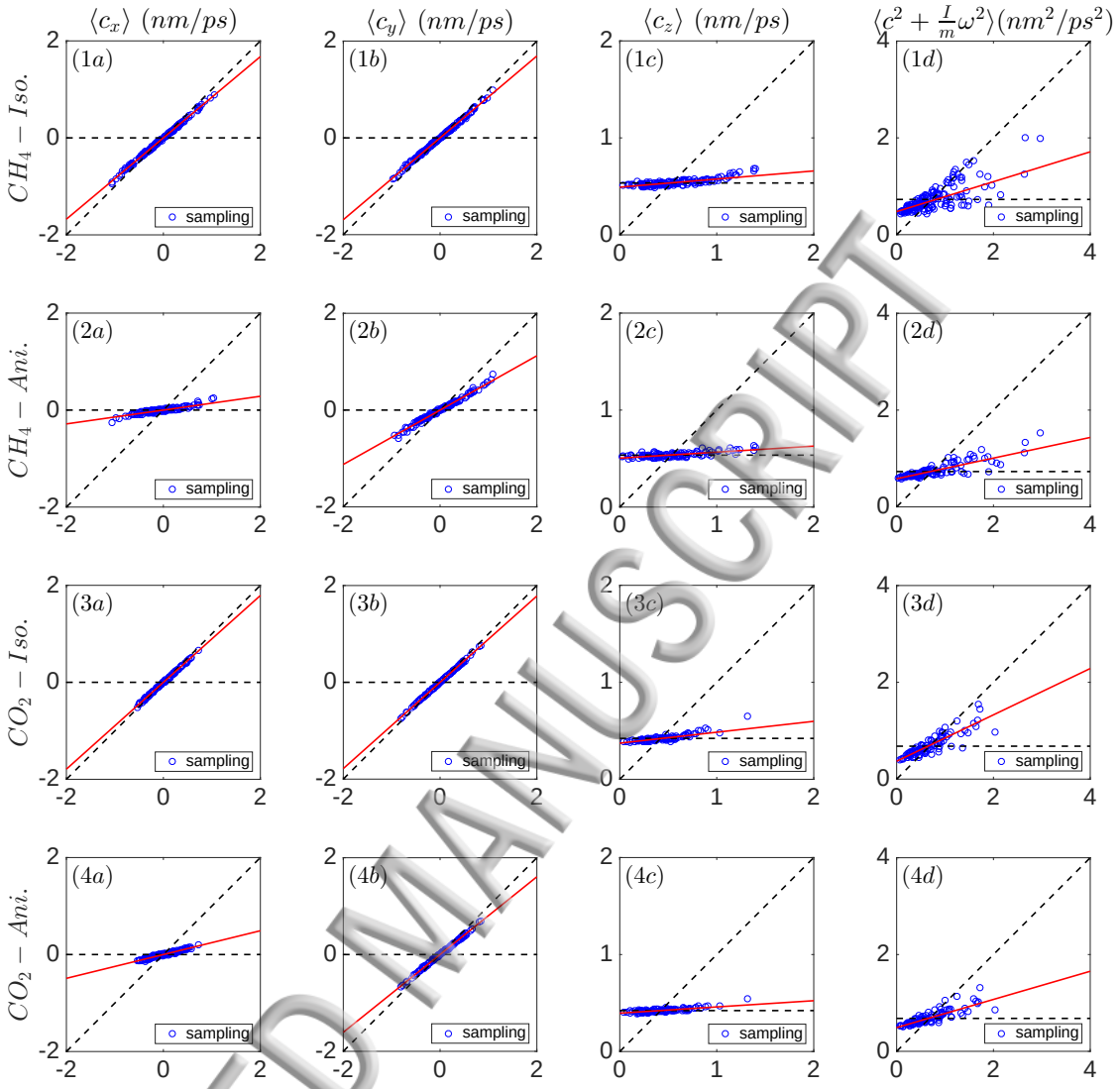

FIG. 3. Correlation analysis using BA scheme for CH_4/CO_2-Graphite. Columns (a), (b), (c) represent the velocity (nm/ps) along x, y, z directions respectively and column (d) the kinetic energy for CH_4 and CO_2 (the prefactor $m/2$ is removed for simplicity). The horizontal axis shows the incident values and the vertical axis the reflection values. The solid lines represent the fit by least squares linear regression using Eq. (13). The diagonal dashed line and the horizontal dashed line indicate the zero accommodation case ($\alpha = 0$) and full accommodation case ($\alpha = 1$), respectively.

smooth graphite surface, the incident and reflected velocity data have significant correlation in x and y directions. Despite its crystalline nature, the surface behavior is isotropic and no visible difference is observed between directions x and y. The accommodation coefficients calculated by the least-squares method [19] in Tab. III also confirm this remark. However, the influence of periodic roughness affects the anisotropy of the surface (second row figures) and the magnitude of the accommodation coefficients. We can see that the scattering is

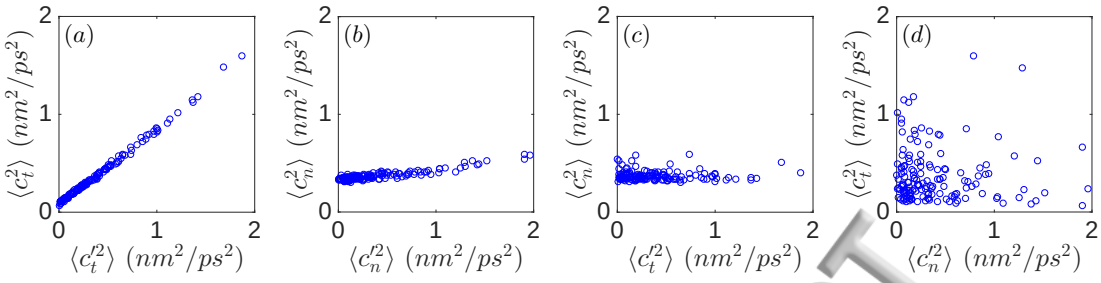

FIG. 4. Detailed analysis of kinetic energy of CH_4 beamed on the smooth surface. The tangential kinetic energy component $c_t^2 = c_x^2 + c_y^2$ and the normal kinetic energy component $c_n^2 = c_z^2$ are used for analysis. Subfigures (a), (b), (c), (d) show the correlation between incident energy and reflective energy components.

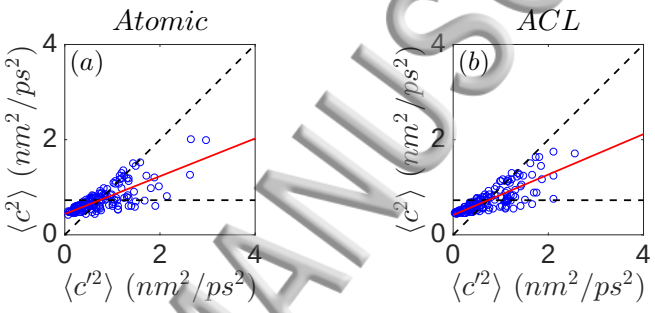

FIG. 5. Energy data scattering observed from (a) MD simulations, (b) parametric ACL model with parameters $\alpha_x = \alpha_y = 0.16$ (constant tangential momentum accommodation coefficient) and $\alpha_z = 0.915$ (constant normal kinetic energy accommodation coefficient)

more diffusive along both directions but more pronounced for x direction. In all cases, the correlation between c_z and c_z' as well as the correlation between c^2 and c'^2 are very weak, and close to the diffusive wall.

We note that all analytical surface models in literature are based on the accommodation coefficients. Thus, we can construct scattering kernels which can serve as boundary conditions for atomistic method like MD or DSMC. The main advantage of these kernels is the simplicity in implementation but theirs drawbacks are their differences from the real surface behavior. This can be explained from the fact that they rely on the existence of the limited number of constant accommodation coefficients. To reconstruct $B(\boldsymbol{\omega}, \boldsymbol{c}|\boldsymbol{\omega}', \boldsymbol{c}')$, we do not use any parameter and make no assumption on the distribution form except for the

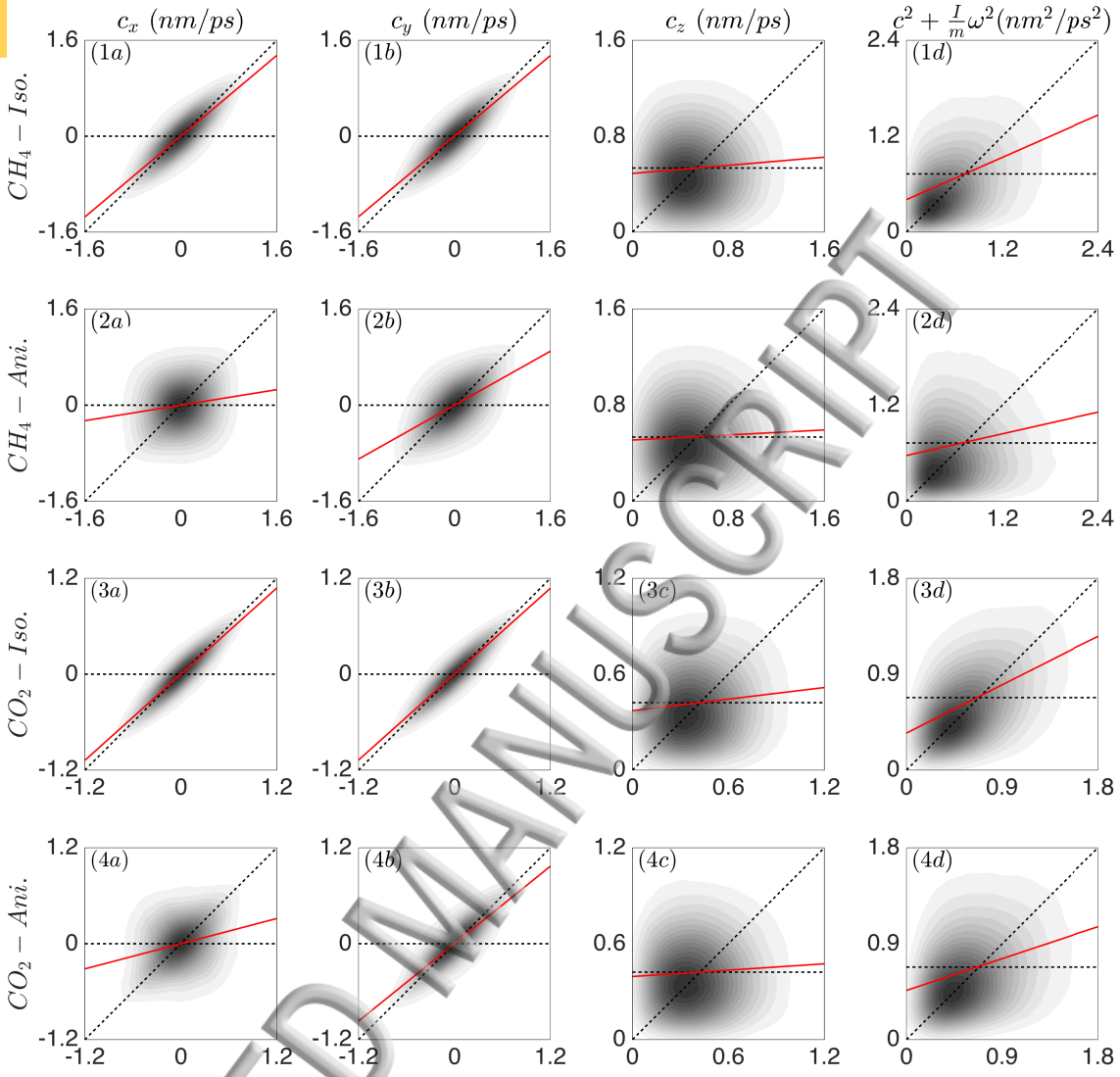

FIG. 6. Collision data of incident and reflected velocities for the CH_4/CO_2-Graphite system. Both stochastic reservoir and graphite wall are maintained at 350 K for CH_4 and 600 K for CO_2. Columns (a), (b), (c) represent the velocity (nm/ps) along directions x, y, z, respectively, and column (d) the kinetic energy for CH_4 and CO_2 (the prefactor $m/2$ is removed for simplicity). The horizontal axis shows the incident values and the vertical axis the reflection values. The solid lines indicate the linear least square fit of incident and reflected values using Eq. (14). The diagonal dashed line and the horizontal dashed line indicate the zero accommodation case ($\alpha = 0$) and full accommodation case ($\alpha = 1$), respectively.

decomposition of each components

$$B(\boldsymbol{\omega}, \boldsymbol{c}|\boldsymbol{\omega}', \boldsymbol{c}') = \prod_{i=1}^{3} B_i(c_i|c_i') B_i^{\omega}(\omega_i|\omega_i'). \tag{33}$$

The above relation reduces the realization of $B(\boldsymbol{\omega}, \boldsymbol{c}|\boldsymbol{\omega}', \boldsymbol{c}')$ to the realizations of independent

Gas	Surface	Scheme	$\alpha_x(c_x)$	$\alpha_y(c_y)$	$\alpha_z(c_z)$	$\alpha_e(c^2+\frac{I}{m}\omega^2)$
CH_4	Isotropic	SE	0.158	0.160	0.915	0.559
		BA	0.162	0.154	0.916	0.691
	Anisotropic	SE	0.839	0.440	0.948	0.775
		BA	0.857	0.438	0.938	0.787
CO_2	Isotropic	SE	0.102	0.104	0.885	0.515
		BA	0.105	0.109	0.888	0.521
	Anisotropic	SE	0.737	0.196	0.942	0.682
		BA	0.755	0.197	0.936	0.709

TABLE III. Accommodation coefficients computed by stochastic equilibrium (SE) simulation method using data of Fig. 6 and by batch average (BA) simulation method in Fig. 3: α_l coefficient is associated to the velocity c_l, α_e is the kinetic energy (the angular velocity of CH_4 is zero).

univariate densities $B_i(c_i|c_i')$ and $B_i^{\omega}(\omega_i|\omega_i')$. We note that, theoretically, the construction of $B(\boldsymbol{\omega}, \boldsymbol{c}|\boldsymbol{\omega}', \boldsymbol{c}')$ doesn't depend on the above assumption. However, the usual non-parametric estimates of multivariate density require a very large number of samples to be accurate (the curse of dimensionality) and more advanced learning methods are needed to solve this issue.

Without losing generality, we take the case of translation velocity c_i. The probability density function (PDF) of reflective velocity with given incident velocity $P(c_i|c_i')$ can be determined by joint PDF of reflective-incident velocity $P(c_i, c_i')$ and marginal PDF of incident velocity $P(c_i')$ with relation:

$$B_i(c_i|c_i') = P(c_i|c_i') = \frac{P(c_i, c_i')}{P(c_i')}. \tag{34}$$

The discrete collision data can be used to estimate the joint probability $P(c_i, c_i')$ by histogram or kernel density estimation method. After determining $B_i(c_i|c_i')$, we can use it to generate the outgoing velocities at any given incident velocities. This can be done via the use of conditional cumulative distribution function (CDF) $F(c_i|c_i')$.

To illustrate the robustness of the non-parametric model, we take the case of anisotropic surface and plot the probability density of input and output velocities of different kernels together with the MD data in Fig. 7. The considered kernels are Dadzie-Meolans (DM) [12] and anisotropic Cercignani-Lampis (ACL) [31], and non-parametric kernel constructed numerically from MD simulations (see Appendix B). The accommodation parameters of

ACL kernel (α_x associated to c_x, α_y to c_y and α_z to c_z^2) and DM kernels (α_x and α_y are the same as ACL kernels and α_z is associated to c_z) are determined by SE simulations using Eq. (14). One can find that the DM kernel that includes mirror-reflected mechanisms is very different from the true collision data, the probability density shows a strong discontinuity. The ACL kernel performs better but the non-parametric kernel is the most faithful to the MD data. Such differences can have significant influences on the results based on the kernel.

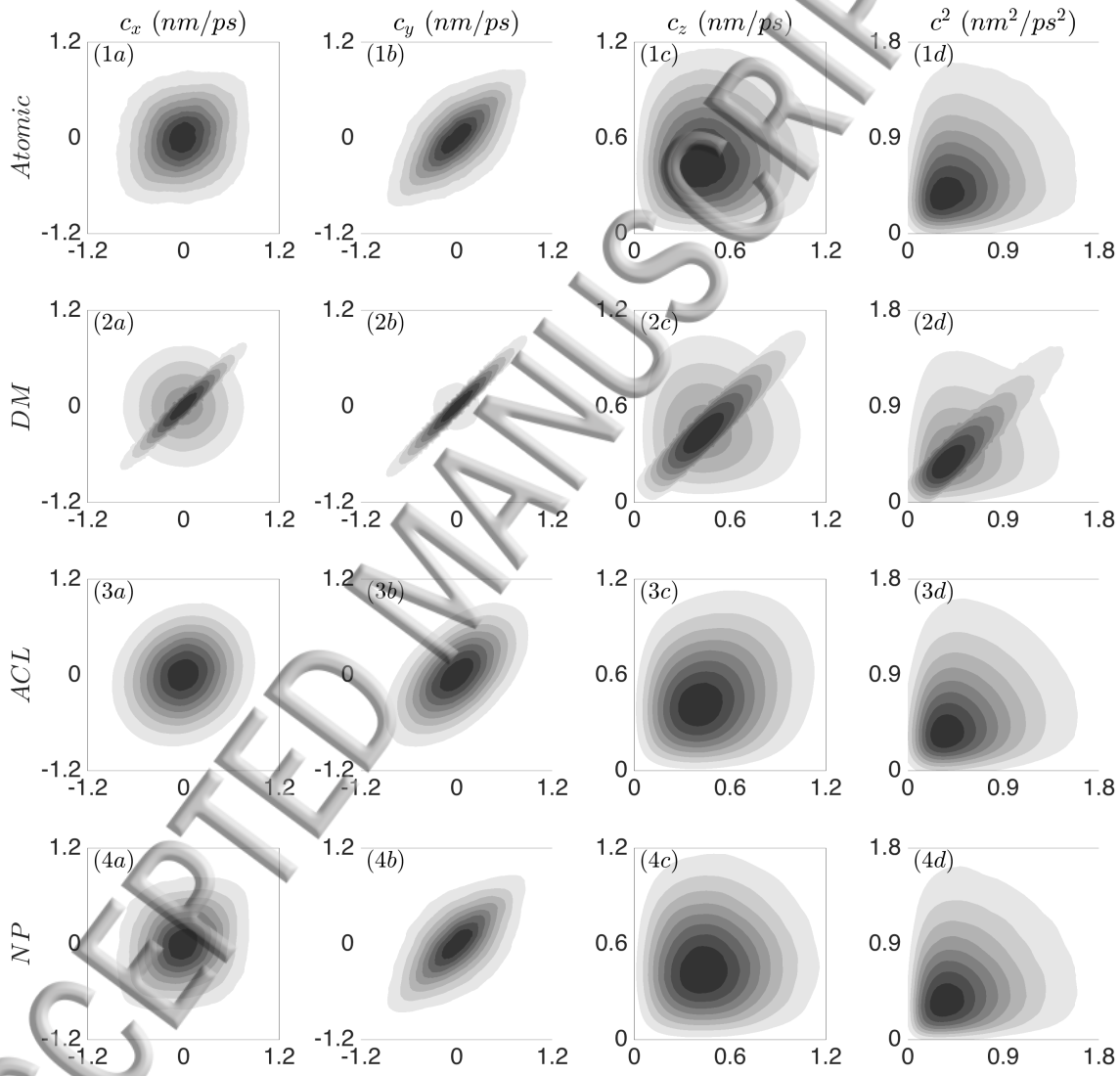

FIG. 7. Velocity probability density of MD simulations and from some scattering kernels: Dadzie-Meolans (DM) [12], Anisotropic Cercignani-Lampis (ACL) [31] and non-parametric (NP) kernel constructed from MD data. The MD data are from collision simulation of CH_4 (350 K) at anisotropic atomic graphite wall (350 K). Columns (a), (b), (c) represent the velocity (nm/ps) at directions x, y, z, respectively, and column (d) the kinetic energy for CH_4 (the prefactor $m/2$ is removed for simplicity). The horizontal axis shows the incident values and the vertical axis the reflection values.

This manuscript was accepted by Phys. Fluids. Click here to see the version of record.

C. Direct computation of interface coefficients

The methods of determining the accommodation parameters like SE and BA depend on the existence of these constant coefficients. The BA gas beam experiments show that the postulates are rather restrictive (see e.g. Fig. 3, column d). Deriving those coefficients by fitting may correspond values in average sense without connection to the boundary conditions (16). Nevertheless, the slip and jump phenomena still exist and it is of interest to identify the coefficients associated to these effects. In this situation, one must make use of the non-equilibrium state of the gas near the wall. In principle, the more realistic the gas distribution is, the better interface coefficients we obtain. Before using more sophisticated distribution like Chapman-Enskog or R13 density, we shall examine the workability of a simpler distribution, MB at different temperatures and mean velocities. For β_{1x}, β_{1y} associated to the friction coefficients, we use Maxwellian with the same temperature as the wall but non zero mean velocity. The latter is a vector lying in the bisector plane (making angle $\pi/4$ with respect to axis x and y) with variable magnitude. For β_2 related to the Kapitza coefficient, we use Maxwellian with zero mean velocity but different temperatures. Specifically, the temperature ranges from 250 K to 450 K for CH_4, from 500 K to 700 K for CO_2 and mean velocities range from -0.05nm/ps to 0.05nm/ps for both CH_4 and CO_2. At this stage, we have two wall models:

- Atomic wall model (AM)
- Non-parametric wall model (NP)

for comparisons. To examine the connection between the quantities in the boundary models, results for the slip velocities, the temperature jump, stress and heat flux obtained by Eqs. (18-23) are plotted together in Fig. 8.

We see a clear linear relation between $-\hat{\sigma}_{kz}$ and $\hat{v}_z$ as well as between $-\hat{q}_z$ and $\Delta\hat{\theta}$ in Fig. 8. The slopes of fitted lines represent the value of the dimensionless friction coefficient β_{1k} (subfigures a and b) and the dimensionless thermal coefficient β_2 (subfigure c). The friction coefficient of the x direction increases 8 times from smooth wall to rough wall, compared with the 3 times increase in the y direction. It's also interesting to see that the β_2

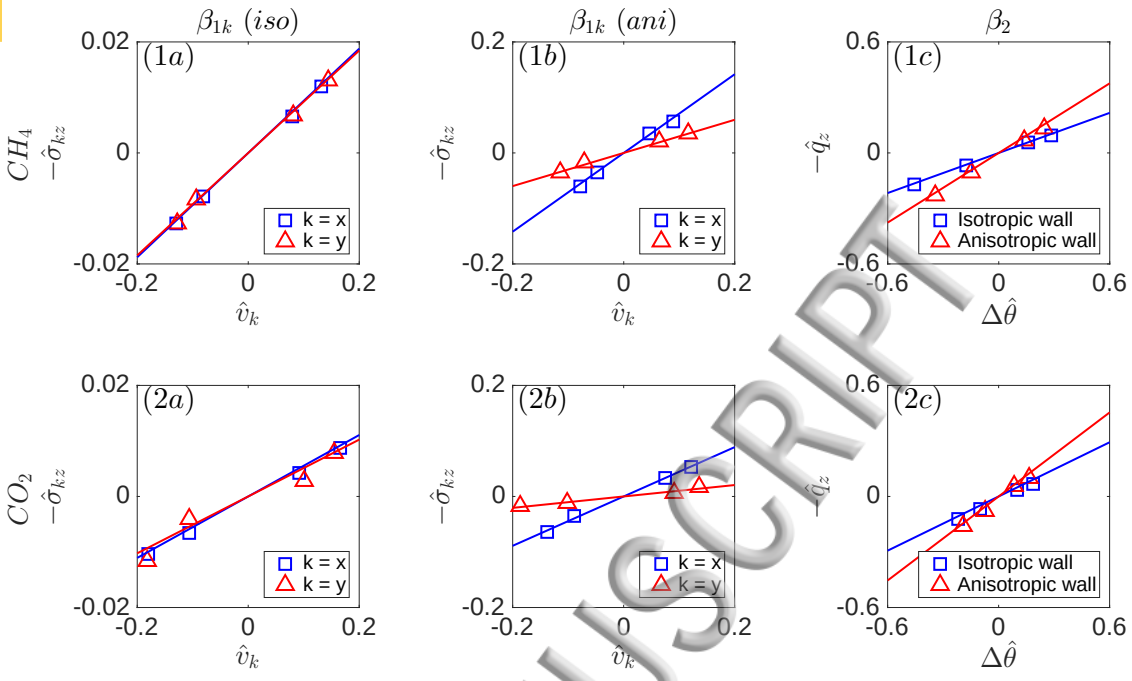

FIG. 8. Method of computing coefficients βs by non-equilibrium simulation, MB distribution and atomic wall model (AM). (a) $-\hat{\sigma}_{kz}$ and $\hat{v}_k$ of the isotropic graphite wall. (b) $-\hat{\sigma}_{kz}$ and $\hat{v}_k$ of the anisotropic graphite wall. (c) $-\hat{q}_z$ and $\Delta\hat{\theta}$ are calculated by incident and reflective velocities on isotropic and anisotropic graphite wall.

coefficient of smooth wall is smaller than the rough wall's (about 2 times). These tendencies coincide with reality that rough surface friction and thermal resistance are larger than the smooth surface ones. For comparison with theoretical models where the accommodation coefficients are connected to the interface equations Eqs. (17), the results of CH_4 and of CO_2 are plotted in Tab. IV.

In terms of friction coefficient β_{1k}, the results of the non-equilibrium method with MB distribution are very close to those obtained with the methods based on equilibrium distribution. This is reasonable since the BA method also shows that the accommodation model works well for this case. For thermal coefficient β_2, the SN method seems to agree better with the coefficient derived from SE method than the BA method. This observation can be explained from the scattering data in the BA method, meaning that the theoretical definition of the thermal accommodation coefficient is no longer valid. In this case, an effective coefficient which reproduces the thermal jump effect can be determined.

Surface	Method	CH_4			CO_2		
		β_{1x}	β_{1y}	β_2	β_{1x}	β_{1y}	β_2
Isotropic	SE (α)	0.087	0.087	0.388	0.054	0.054	0.347
	SN (MB-AM)	0.093	0.093	0.361	0.053	0.053	0.488
	SN (MB-NP)	0.095	0.095	0.382	0.052	0.052	0.469
	SN (CE-NP)	0.094	0.094	0.336	-	-	-
Anisotropic	SE (α)	0.722	0.282	0.632	0.584	0.108	0.518
	SN (MB-AM)	0.709	0.299	0.627	0.444	0.103	0.756
	SN (MB-NP)	0.720	0.298	0.644	0.459	0.102	0.728
	SN (CE-NP)	0.646	0.280	0.553	-	-	-

TABLE IV. The β coefficients of CH_4 and CO_2 computed by SN methods and compared with values obtained from accommodation coefficients (SE method, Tab. III) via formula $\beta_{1k} = \alpha_k/(2-\alpha_k)$, $\beta_2 = \alpha_e/(2-\alpha_e)$. MB: Maxwell-Boltzmann distribution, CE: Chapman-Enskog distribution, AM: atomic model for wall, NP: the wall is modeled by non-parametric scattering kernel $B(\boldsymbol{c}|\boldsymbol{c}')$, instead of atomic wall (as in MB-AM method). To increase the precision of the slip coefficients for smooth (isotropic) surface, we average values along β_{1x} and β_{1y}.

D. Influences of non-equilibrium distributions and discussion

Essentially based on the same procedure as previous subsection, we study the influence of the near wall distribution and the surface models on the interface coefficients. We focus on the monatomic gas CH_4, NP wall model and the following non-equilibrium distributions:

- Chapman-Enskog distribution
- R13 distribution

To generate CE and R13 distributions, we use the Acceptance-Rejection approach described in Appendix A. In addition to temperature and mean velocity, the CE and R13 distributions require input fluxes and moments which are generally unknown. We carry out the following iterations:

- Step n

  - Generation of input distribution using CE (or R13) distribution with average moments of the previous steps $n-1$.
  - Compute the output distribution using the kernel $B(\boldsymbol{c}|\boldsymbol{c}')$.
  - Calculate the average moments at the wall from input and output distributions.
  - Next step.

The loop stops when all the average moments converge (see e.g Fig. 9). The input

distribution at the first step $n = 1$ can be initialized with MB distribution as the previous SN/MB scheme, i.e all fluxes (heat fluxes, stress, etc...) are set zero. The latter quantities become non-zero after the initialization ($n \geq 2$) and we can effectively use the CE and R13 generator. Numerical tests show that while the average moments at convergence depend on the initialized values, the value of β coefficients are insensitive to them.

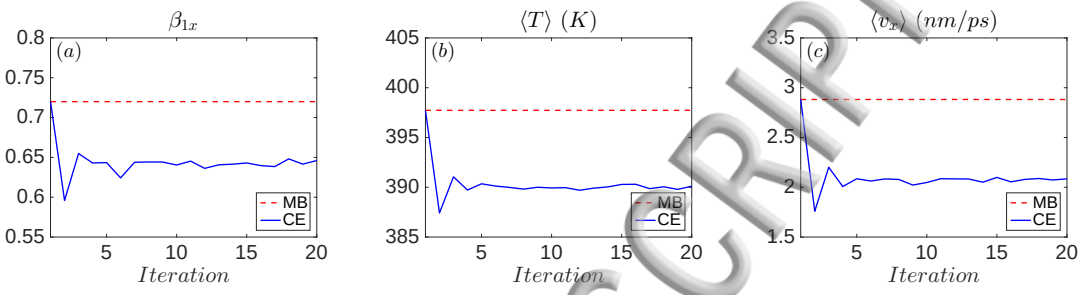

FIG. 9. Convergence test of CE-NP kernel iteration for rough anisotropic surface. Subfigures (a): Friction coefficient β_{1x}, (b) Gas temperature (c) Gas velocity.

About 10^7 collisions with scattering kernel are simulated. In Tab. IV, we find that all the methods yield results close to each other, especially for isotropic surface. For anisotropic surface and friction coefficient along x, the method based on CE shows some discrepancies with the rest (although the coefficient is of the same range of order). The visible differences can be explained from the influences of heat flux and shear stress at convergence. By examining in detail the convergence of β_{1x} in Fig. 9, we find the final parameter is different from the first iteration one. It is suggested that the presence of the roughness perturbs considerably the phase density. Due to the realistic kernel $B(\boldsymbol{c}|\boldsymbol{c}')$, the output is not necessarily of the same distribution class as the input. This raise questions on the use of CE distribution near the wall, especially the component c_x along the roughness directions. Another possible reason is that there may be a considerable coupling between different moments which must be taken into account in the phenomenological equations. The complete answer can only be found from flow simulations using the same surface model, but with different input distributions.

Next we consider another non-equilibrium distribution associated to R13 moment equations. The boundary conditions are originally derived for Maxwell scattering kernel with one accommodation coefficient (isotropic surface) and all β coefficients being identical. In

In order to test the R13 generator, we use first the Maxwell kernel with $\alpha = 0.3$ and obtain interface coefficients. From Tab. IV, we find that these coefficients are overall in good agreement with the theory prediction $\beta = \alpha/(2-\alpha) = 0.176$. Most of the computed coefficients are within less than 1% error from the analytical value. This is a good starting point to proceed with our graphite surface.

We use NP model for our graphite surface. The results show that coefficients β_1, β_2 agree with the computed values for NSF equations listed in Tab. V. Coefficients $\beta_3, \beta_4, \beta_5$ correspond to boundary conditions for higher order terms. As the overall remark, all coefficients β are different, showing that the use of Maxwell kernel cannot capture correctly the boundary conditions at the wall. In this case, the present approach can provide an alternative and reliable solution for any surface.

Surface	Kernel	β_1	β_2	β_3	β_4	β_5
Test	Maxwell	0.177	0.177	0.160	0.173	0.161
Graphite	NP	0.097	0.373	0.024	0.028	0.129

TABLE V. β coefficients of R13 equations using Maxwell kernel ($\alpha = 0.3$) and non-parametric scattering kernel.

IV. CONCLUSIONS

It is known that gas flows at high Knudsen number are present in micro-nanopore underground. To accurately obtain macroscopic transport behavior (permeability for example), we must use relevant gas model and boundary conditions at the pore scale. The present paper is devoted to the construction of gas-wall interaction models and to the determination of boundary conditions for continuum equations such as Navier-Stokes-Fourier or R13 equations.

Based on MD simulation of independent collisions of CH_4 and CO_2 rigid molecules on graphite surface, we collect data of pre- and post-collision and numerically recover the scattering kernel for the gas-wall couples. Specifically, it can be used to construct non-parametric models capable of generating a distribution of post-collision velocity, given the pre-collision velocity. The effective accommodation coefficients can also be obtained from

ing scattering kernel using a different fitting procedure.

In the general case, a method is proposed to directly compute the parameters of any phenomenological boundary conditions without using the concept of accommodation coefficients. The approach relies on the general scattering kernel issued from MD with suitable input gas distribution, which is similar to the theoretical method of Grad [24]. Such an approach is of interest since it can capture more accurately the distribution of reflection velocity. There are still some drawbacks to the current version which will be improved in the future, for example, the use of rigid gas molecule model and the assumptions of independence between the velocity components. Another interesting subject which has not been treated in this work is the Knudsen layer effect. We note that by simulating flows using non-parametric kernel, one can obtain correction coefficients to the microslip obtained by the present paper.

APPENDIX

A. Generation of non-equilibrium distribution

Generating pre-collision velocity of particle requires first the PDF of initial velocity. The Maxwell-Boltzmann distribution is used for a equilibrium dilute gas at temperature T. In order to generate the pre-collision velocity, we rewrite the flux associated to the normalized MB distribution $f_M^*(\tilde{\boldsymbol{C}})$ as:

$$f_M^*(\tilde{\boldsymbol{C}}) = 2\frac{|\tilde{C}_z|}{\pi}\exp\left(-\tilde{\boldsymbol{C}}^2\right), \quad \tilde{C}_z < 0, \tag{35}$$

where $\tilde{\boldsymbol{C}} = \boldsymbol{C}/\sqrt{2\theta}$ and $\theta = k_B T/m$. This distribution is constituted of three independent distributions: two normal distributions along x, y and a Rayleigh distribution along z. Then we can calculate the flux associated to Chapman-Enskog distribution $f_{CE}^*(\tilde{\boldsymbol{C}})$ by the relation:

$$f_{CE}^*(\tilde{\boldsymbol{C}}) = \Gamma_{CE}(\tilde{\boldsymbol{C}}) f_M^*(\tilde{\boldsymbol{C}}), \quad \tilde{C}_z < 0, \tag{36}$$

where

$$\begin{aligned}\Gamma_{CE}(\tilde{\boldsymbol{C}}) = 1+&\left(\tilde{q}_x\tilde{C}_x+\tilde{q}_y\tilde{C}_y+\tilde{q}_z\tilde{C}_z)(\frac{2}{5}\tilde{C}^2-1)\right)\\ &+2\left(\tilde{\sigma}_{xy}\tilde{C}_x\tilde{C}_y+\tilde{\sigma}_{xz}\tilde{C}_x\tilde{C}_z+\tilde{\sigma}_{yz}\tilde{C}_y\tilde{C}_z\right)\\ &+\tilde{\sigma}_{xx}\tilde{C}_x^2+\tilde{\sigma}_{yy}\tilde{C}_y^2+\tilde{\sigma}_{zz}\tilde{C}_z^2,\end{aligned} \tag{37}$$

with

$$\tilde{\sigma}_{ij}=\frac{\sigma_{ij}}{p},\quad \tilde{q}_i=\frac{q_i}{p\sqrt{\theta/2}},\quad p=mn\theta,\quad i,j=x,y,z. \tag{38}$$

Similarly, the R13 distribution can be calculated from MB distribution by the relation:

$$f^*_{R13}(\tilde{\boldsymbol{C}})=\Gamma_{R13}(\tilde{\boldsymbol{C}})f^*_M(\tilde{\boldsymbol{C}}),\quad \tilde{C}_z<0, \tag{39}$$

where

$$\begin{aligned}&\Gamma_{R13}(\tilde{\boldsymbol{C}})=1+\varphi_{13}(\tilde{\boldsymbol{C}})+\varphi_{R1}(\tilde{\boldsymbol{C}})+\varphi_{R2}(\tilde{\boldsymbol{C}}),\\ &\varphi_{13}(\tilde{\boldsymbol{C}})=\left(\tilde{q}_x\tilde{C}_x+\tilde{q}_z\tilde{C}_z\right)\left(\frac{2}{5}\tilde{C}^2-1\right)+2\tilde{\sigma}_{xz}\tilde{C}_x\tilde{C}_z+\tilde{\sigma}_{xx}\tilde{C}_x^2+\tilde{\sigma}_{yy}\tilde{C}_y^2+\tilde{\sigma}_{zz}\tilde{C}_z^2,\\ &\varphi_{R1}(\tilde{\boldsymbol{C}})=\frac{1}{3}\left(\tilde{m}_{xxx}\tilde{C}_x^3+\tilde{m}_{zzz}\tilde{C}_z^3\right)+\tilde{m}_{xxz}\tilde{C}_x^2\tilde{C}_z+\tilde{m}_{xzz}\tilde{C}_x\tilde{C}_z^2+\tilde{m}_{xyy}\tilde{C}_x\tilde{C}_y^2+\tilde{m}_{zyy}\tilde{C}_z\tilde{C}_y^2,\\ &\varphi_{R2}(\tilde{\boldsymbol{C}})=\left(\tilde{R}_{xx}\tilde{C}_x^2+\tilde{R}_{yy}\tilde{C}_y^2+\tilde{R}_{zz}\tilde{C}_z^2+2\tilde{R}_{xy}\tilde{C}_x\tilde{C}_y\right)\left(\frac{\tilde{C}^2}{7}-\frac{1}{2}\right)+\frac{\tilde{R}}{30}\left(\tilde{C}^4-5\tilde{C}^2+\frac{15}{4}\right),\end{aligned} \tag{40}$$

with

$$\tilde{m}_{ijl}=\frac{m_{ijl}}{p\sqrt{\theta/2}},\quad \tilde{R}_{ij}=\frac{R_{ij}}{p\theta},\quad \tilde{R}=\frac{R}{p\theta}\quad i,j,l=x,y,z. \tag{41}$$

Since the CE and R13 distributions have analytical PDF expression, we can generate random velocities corresponding to these distributions by the Acceptance-Rejection method. The specific steps are as follows:

1. Find $B_{CE}=\max(|\sigma_{ij}|,|q_i|)$ for distribution CE, $B_{R13}=\max(|\sigma_{ij}|,|q_i|,|m_{ijk}|,|R_{ij}|,|R_{ij}|)$ for distribution R13 .

2. Set amplitude parameter $A_{CE}=1+30B_{CE}$ and $A_{R13}=1+60B_{R13}$.

3. Generate a normalized velocity $\tilde{\boldsymbol{C}}_{MB}$ obeying MB distribution (Eq. (35)), and a uniform random number $U(0,1)$.

4. If $\Gamma_{CE}(\tilde{\boldsymbol{C}}_{MB}) \geq AU$, accept $\tilde{\boldsymbol{C}}_{MB}$ as normalized CE distribution velocity $\tilde{\boldsymbol{C}}_{CE}$, and if $\Gamma_{R13}(\tilde{\boldsymbol{C}}_{MB}) \geq AU$, accept $\tilde{\boldsymbol{C}}_{MB}$ as normalized R13 distribution velocity $\tilde{\boldsymbol{C}}_{R13}$; else reject this velocity and return to step 3;

5. The real velocity is $\boldsymbol{c} = \sqrt{2\theta}\tilde{\boldsymbol{C}}_{MB} + \boldsymbol{v}$, $\boldsymbol{v}$ is the mean velocity.

During the Acceptance-Rejection process, the function $\Gamma(\tilde{\boldsymbol{C}})$ can be negative. This velocity is rejected in this case.

B. Method for generating non-parametric kernel

Different from parametric scattering models, like CL or Maxwell, the non-parametric wall model is not specified a priori but is instead determined from data. Using the discrete incident-reflection velocities data, we can generate the reflective velocities at any given incident velocities. The implementation of Eq. (34) is as follows:

1. Discretize the velocity space c_i' and c_i to a series of velocity points with sufficient small interval. Choose a volume $\Delta c_i'$ and let us call class c_i' the collisions in the volume centered at c_i'.

2. Use sliding window method to count the number of collision ΔN in class c_i' .

3. Calculate discrete CDF of every class c_i' as $F(x|c_i') = \dfrac{\Delta N(c_i \leq x)}{\Delta N}$.

4. Generate a uniform random number U between 0 to 1, then the reflective velocity is $c_i \sim F^{-1}(U|c_i')$.

The procedure is shown in Fig. 10. The reflective rotation velocity can be obtained by the same procedure.

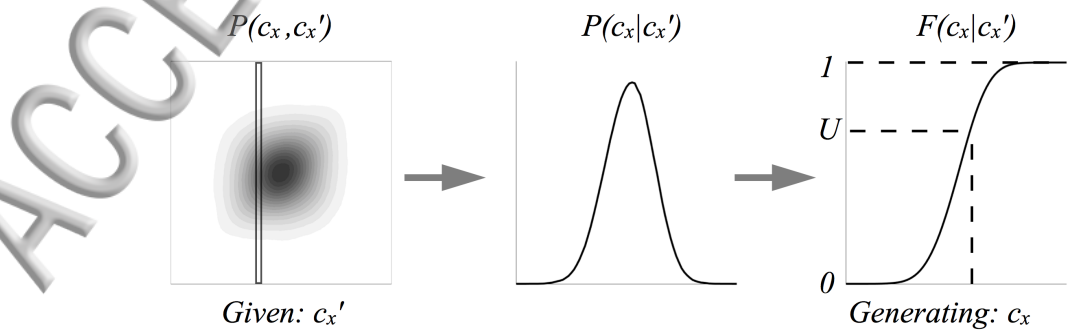

FIG. 10. Generation of velocity using non-parametric kernel derived from MD collision clouds

ACKNOWLEDGMENTS

We thank Prof. Christophe Desceliers for his advice regarding probability calculation. Discussions with Prof. Christian Soize were appreciated.

[1] L. Klinkenberg *et al.*, in *Drilling and production practice* (American Petroleum Institute, 1941).

[2] A. S. Ziarani and R. Aguilera, Transport Porous Med. **91**, 239 (2012).

[3] M. Torrilhon, Annu. Rev. Fluid Mech **48**, 429 (2016).

[4] H. Struchtrup, *Macroscopic Transport Equations for Rarefied Gas Flows: Approximation Methods in Kinetic Theory* (Springer, 2005).

[5] M. Liao, Q. D. To, C. Léonard, V. Monchiet, and V. H. Vo, J. Chem. Phys. **146**, 014707 (2017).

[6] J.-L. Barrat and L. Bocquet, Phys. Rev. Lett. **82**, 4671 (1999).

[7] L. Bocquet and J.-L. Barrat, Phys. Rev. E **49**, 3079 (1994).

[8] J. Maxwell, Philos. T R. Soc. A **170**, 231 (1879).

[9] C. Cercignani and M. Lampis, Transport Theory Stat. Phys. **1**, 101 (1971).

[10] C. Cercignani, *Rarefied gas dynamics: from basic concepts to actual calculations*, Vol. 21 (Cambridge University Press, 2000).

[11] K. Yamamoto, H. Takeuchi, and T. Hyakutake, Phys. Fluids **18**, 046103 (2006).

[12] S. K. Dadzie and J. G. Méolans, J. Math. Phys. **45**, 1804 (2004).

[13] M. Hossein Gorji and P. Jenny, Phys. Fluids **26**, 122004 (2014).

[14] Q. D. To, V. H. Vu, G. Lauriat, and C. Léonard, J. Math. Phys. **56**, 103101 (2015).

[15] J. C. Tully, J. Chem. Phys. **92**, 680 (1990).

[16] T. Yan, W. L. Hase, and J. C. Tully, J. Chem. Phys. **120**, 1031 (2004).

[17] T. Liang, Q. Li, and W. Ye, J. Comput. Phys. **352**, 105 (2017).

[18] S. K. Dadzie and J. G. Méolans, Physica A **358**, 328 (2005).

[19] P. Spijker, A. J. Markvoort, S. V. Nedea, and P. A. J. Hilbers, Phys. Rev. E **81**, 011203 (2010).

[20] M. Torrilhon and H. Struchtrup, J. Comput. Phys. **227**, 1982 (2008).

[21] H. Struchtrup, Continuum Mech. Therm. **17**, 43 (2005).

[22] H. Struchtrup and M. Torrilhon, Phys. Fluids **15**, 2668 (2003).

[23] S. Chapman and T. Cowling, *The mathematical theory of non-uniform gases: an account of the kinetic theory of viscosity, thermal conduction, and diffusion in gases* (Cambridge University

Press, 1970).

[24] H. Grad, in *Thermodynamik der Gase/Thermodynamics of Gases* (Springer, 1958) pp. 205–294.

[25] A. L. Garcia and B. J. Alder, J. Comput. Phys. **140**, 66 (1998).

[26] S. Plimpton, J. Comput. Phys. **117**, 1 (1995).

[27] S. J. Stuart, A. B. Tutein, and J. A. Harrison, J. Chem. Phys. **112**, 6472 (2000).

[28] Z. Zhang and S. C. Glotzer, Nano Letters **4**, 1407 (2004).

[29] P. J. Linstrom and M. W. G., NIST Chemistry WebBook; NIST Standard Reference Database No. 69 (2017).

[30] T. T. Pham, Q. D. To, G. Lauriat, C. Léonard, and V. Van Hoang, Phys. Rev. E **86**, 051201 (2012).

[31] Q. D. To, V. H. Vu, G. Lauriat, and C. Léonard, in *ASME 2016 14th International Conference on Nanochannels, Microchannels, and Minichannels collocated with the ASME 2016 Heat Transfer Summer Conference and the ASME 2016 Fluids Engineering Division Summer Meeting* (American Society of Mechanical Engineers, 2016) pp. V001T01A002–V001T01A002.

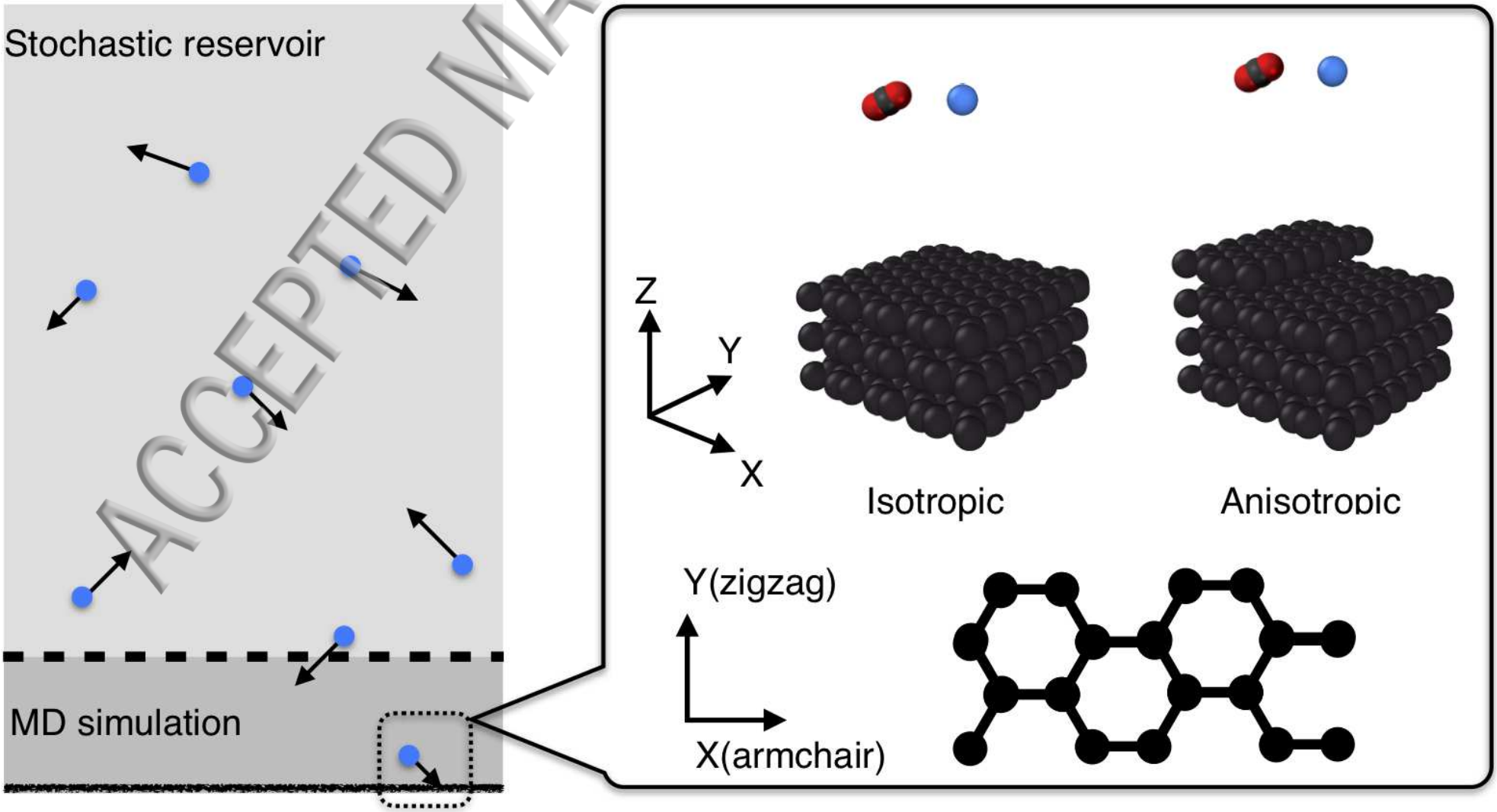
Stochastic reservoir
MD simulation
Z
Y
X
Isotropic
Anisotropic
Y(zigzag)
X(armchair)

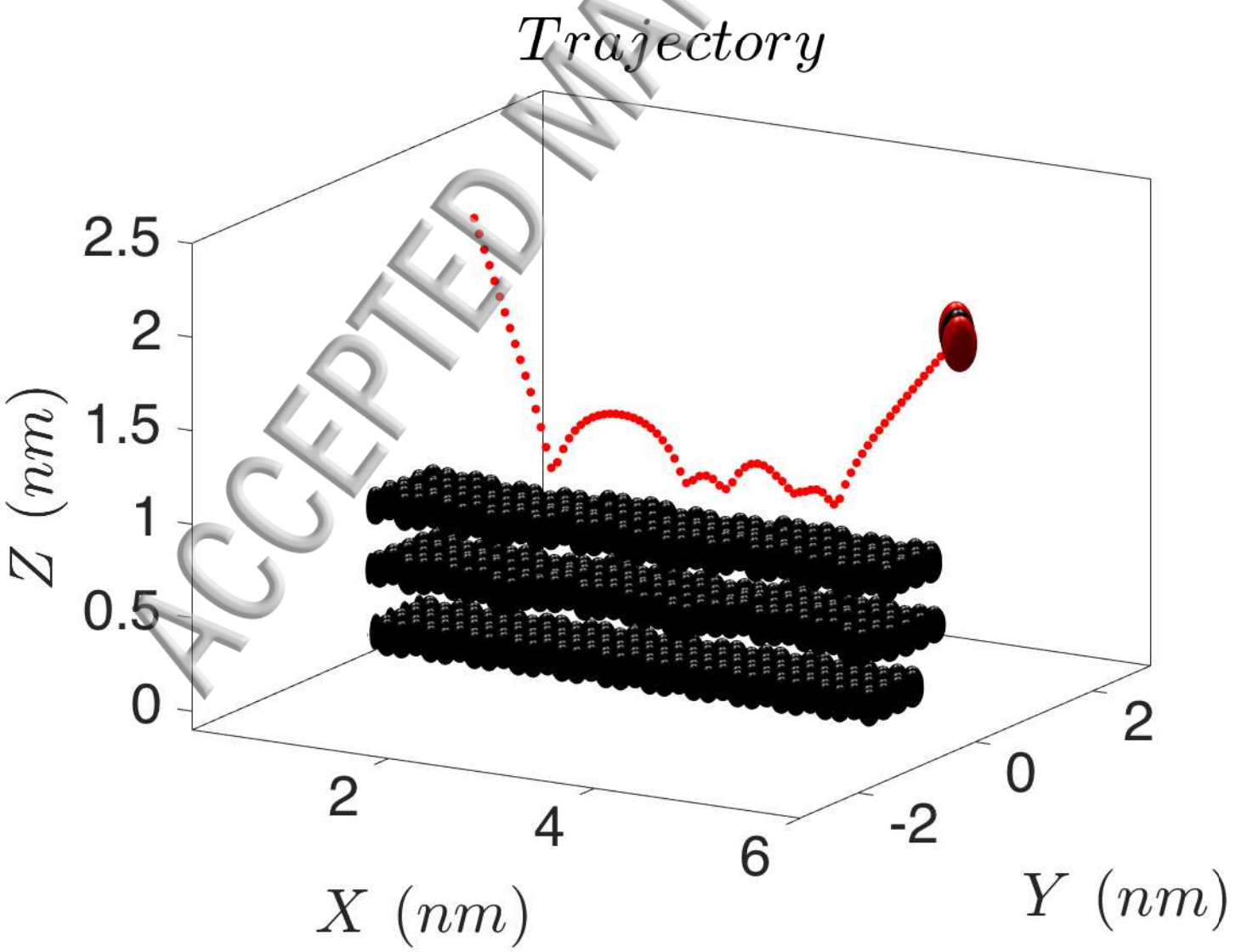

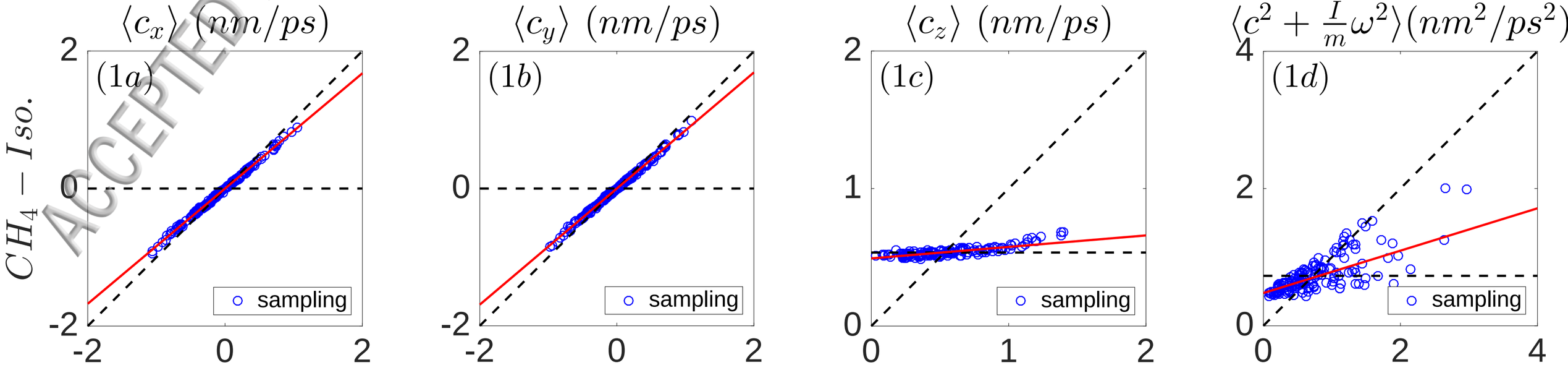
$\langle c_x \rangle\ (nm/ps)$
$\langle c_y \rangle\ (nm/ps)$
$\langle c_z \rangle\ (nm/ps)$
$\langle c^2 + \frac{I}{m}\omega^2 \rangle (nm^2/ps^2)$
$CH_4 - Iso.$
(1a)
(1b)
(1c)
(1d)
sampling
sampling
sampling
sampling

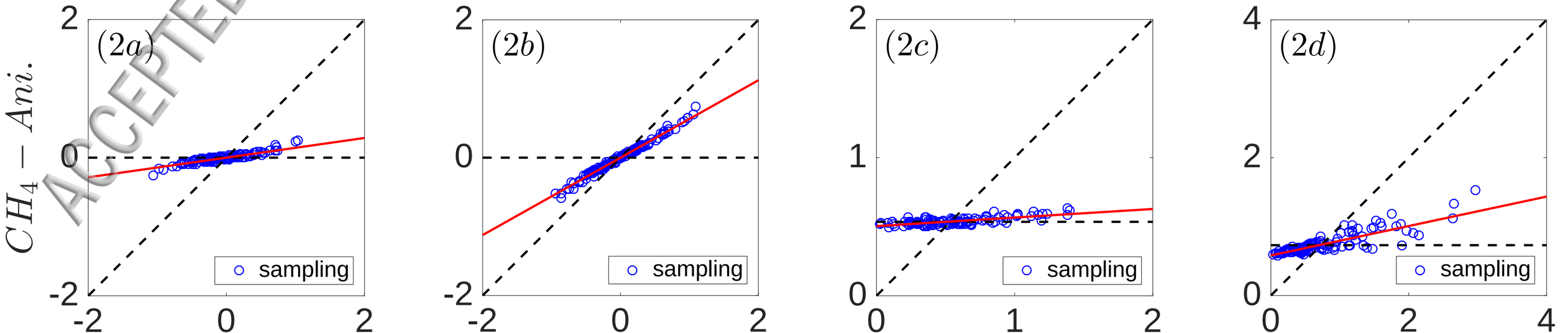
$CH_4 - Ani.$
(2a)
(2b)
(2c)
(2d)
sampling
sampling
sampling
sampling
2
0
-2
-2
0
2
2
0
-2
-2
0
2
2
1
0
0
1
2
4
2
0
0
2
4

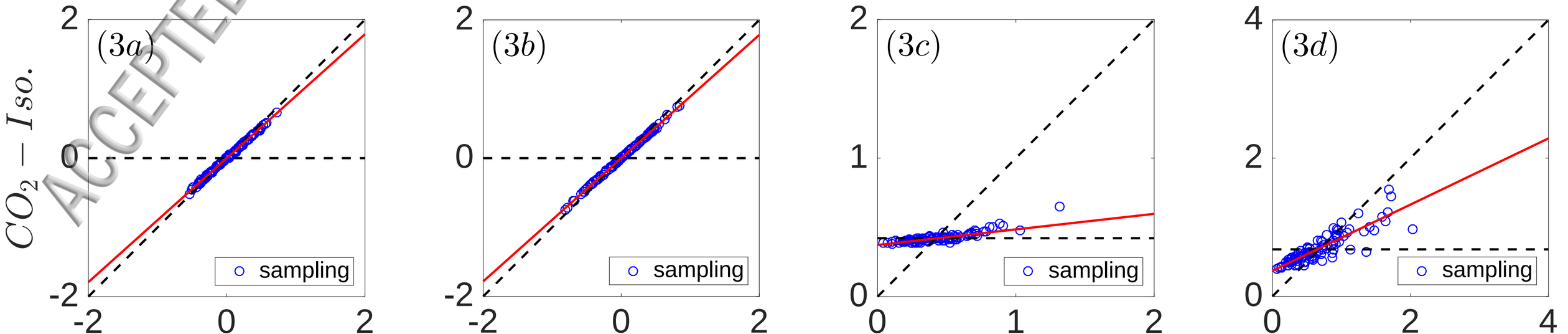
$CO_2 - Iso.$
(3a)
(3b)
(3c)
(3d)
sampling
sampling
sampling
sampling
2
0
-2
-2
0
2
2
0
-2
-2
0
2
2
1
0
0
1
2
4
2
0
0
2
4

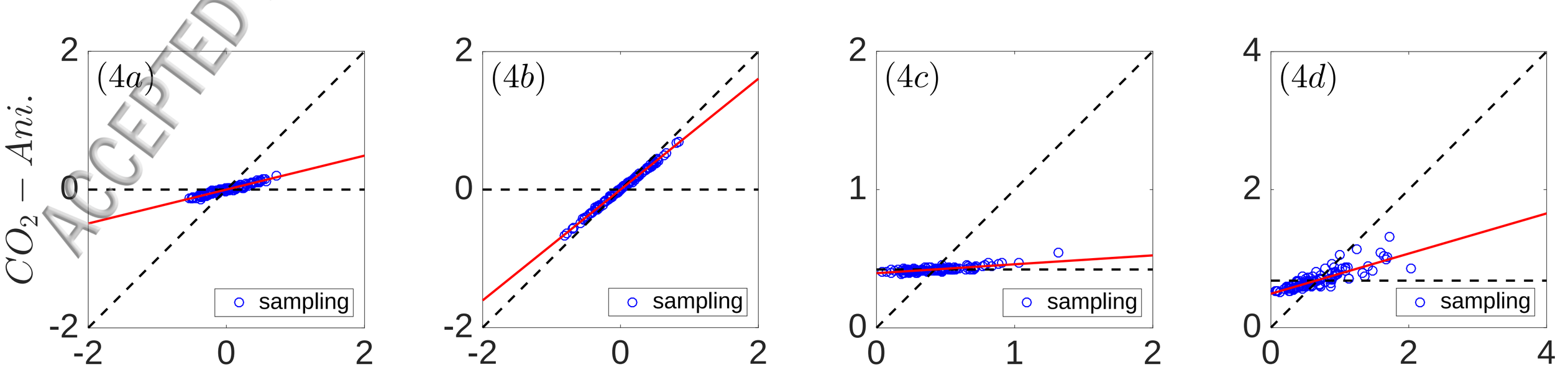
$CO_2 - Ani.$
(4a)
(4b)
(4c)
(4d)
sampling
sampling
sampling
sampling
2
0
-2
-2
0
2
2
0
-2
-2
0
2
2
1
0
0
1
2
4
2
0
0
2
4

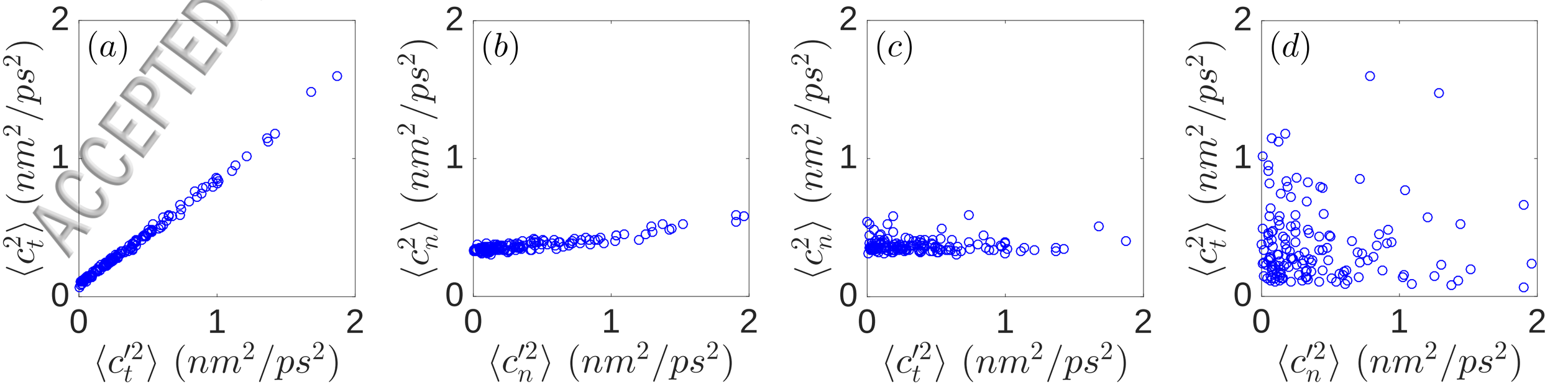
(a)
(b)
(c)
(d)
$\langle c_t^2 \rangle$ (nm^2/ps^2)
$\langle c_n^2 \rangle$ (nm^2/ps^2)
$\langle c_t'^2 \rangle$ (nm^2/ps^2)
$\langle c_n'^2 \rangle$ (nm^2/ps^2)
0
1
2

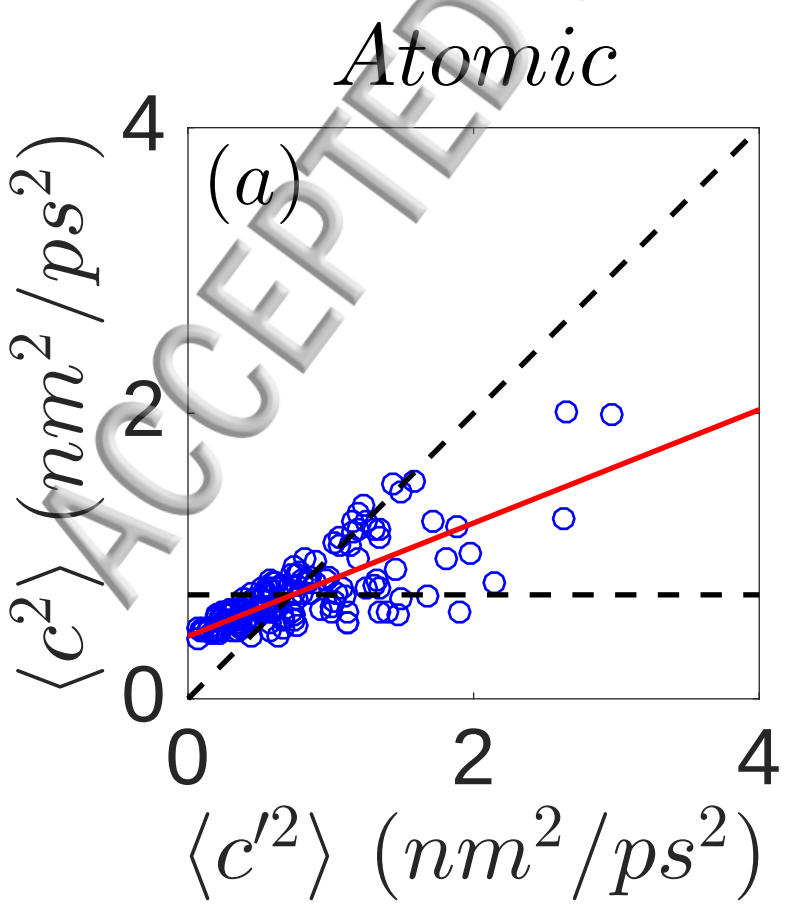
Atomic
(a)
$\langle c^2 \rangle \ (nm^2/ps^2)$
$\langle c'^2 \rangle \ (nm^2/ps^2)$
0
2
4
0
2
4

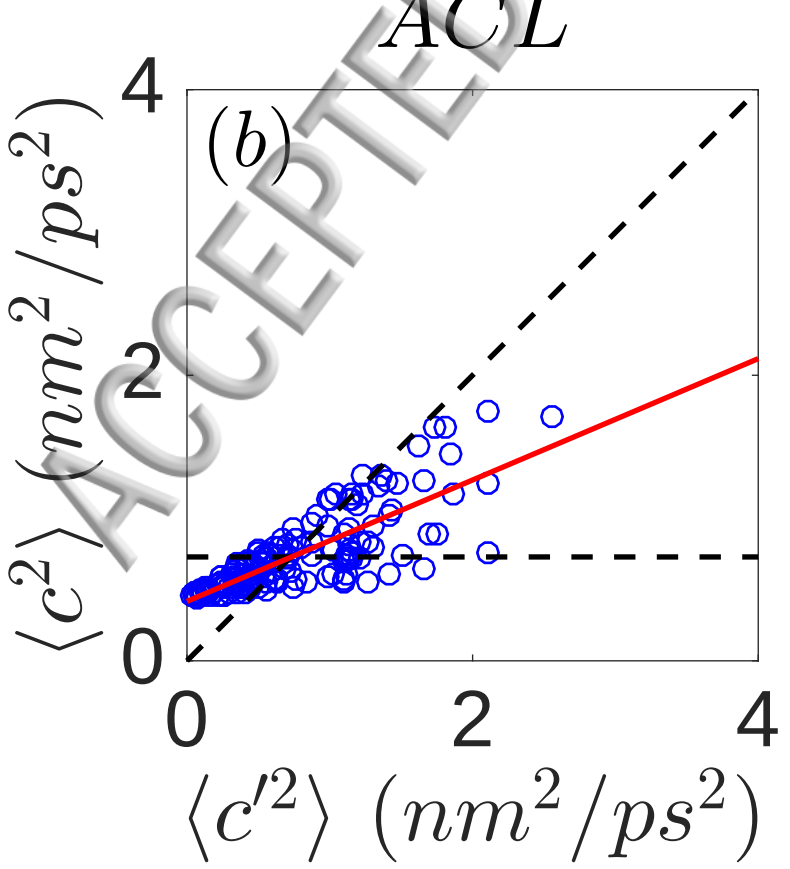
ACL
(b)
4
2
0
0
2
4
$\langle c^2 \rangle$ (nm^2/ps^2)
$\langle c'^2 \rangle$ (nm^2/ps^2)

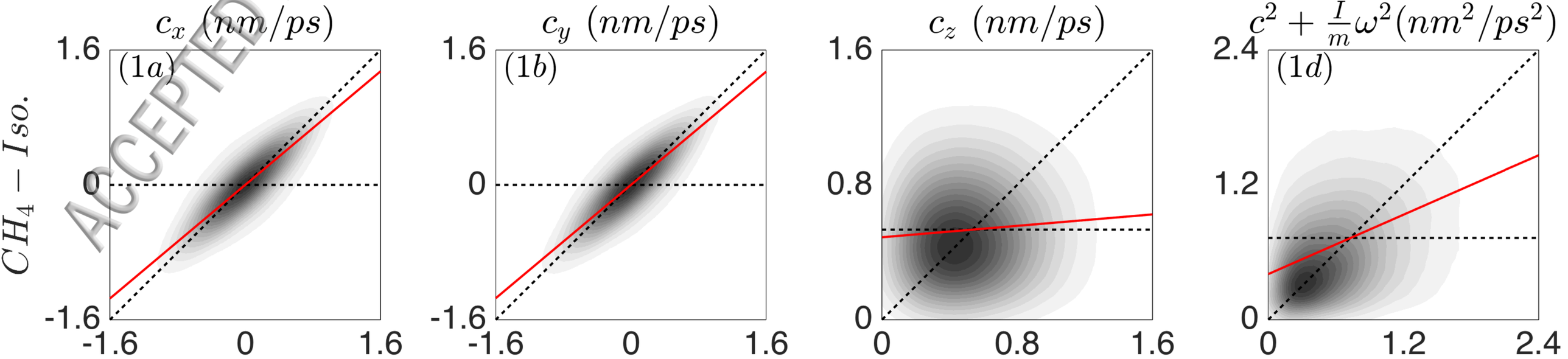
$c_x\ (nm/ps)$
$c_y\ (nm/ps)$
$c_z\ (nm/ps)$
$c^2 + \frac{I}{m}\omega^2 (nm^2/ps^2)$
$CH_4 - Iso.$
(1a)
(1b)
(1d)
1.6
0
-1.6
0.8
2.4
1.2

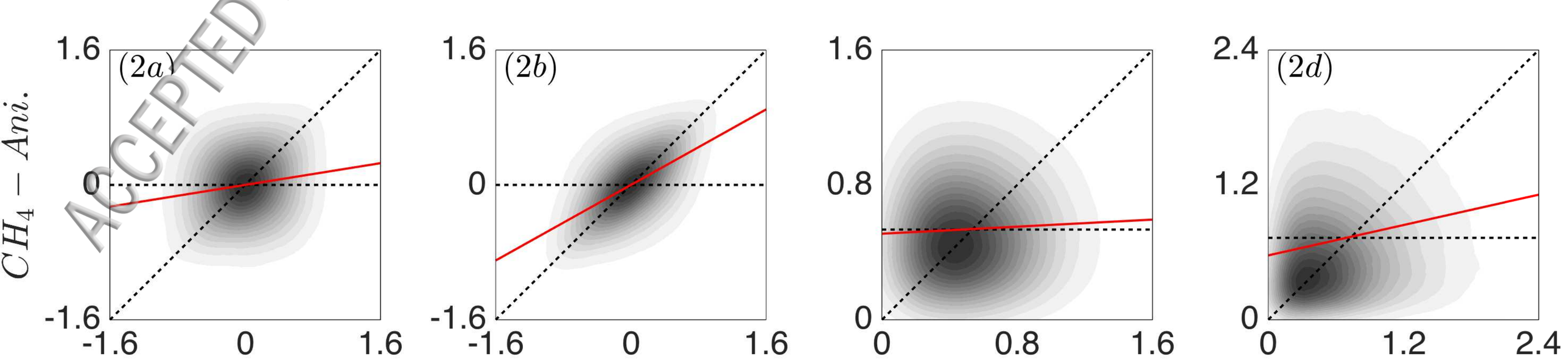

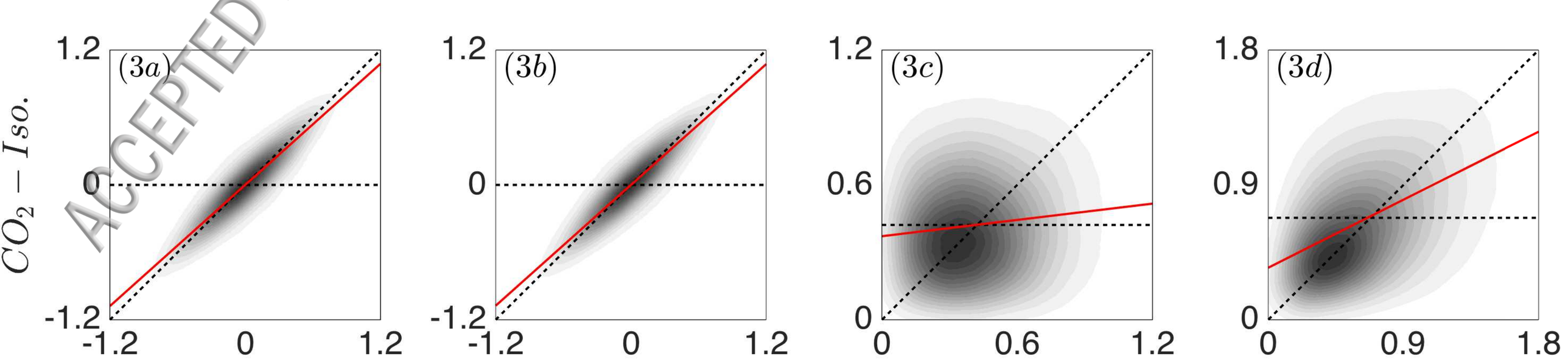

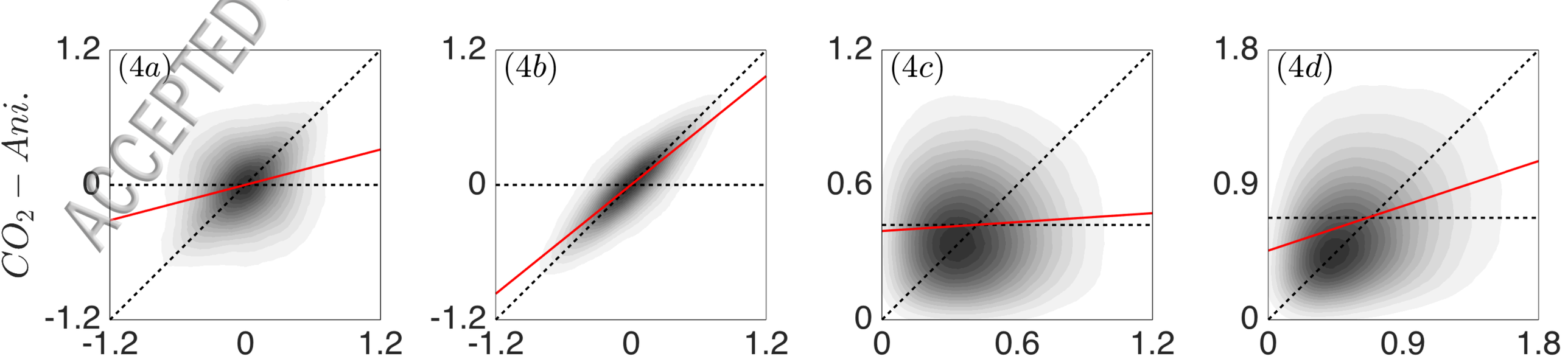

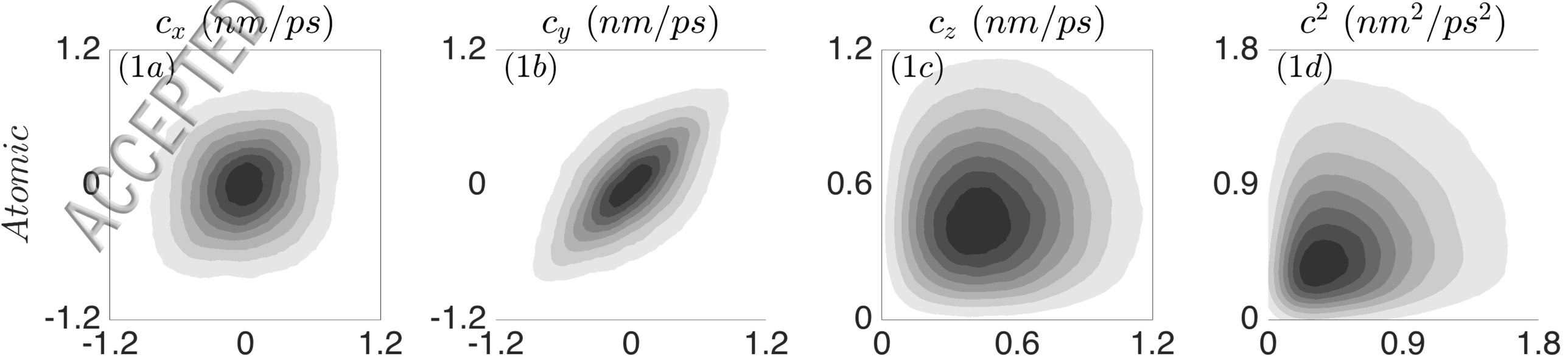
$c_x\ (nm/ps)$
$c_y\ (nm/ps)$
$c_z\ (nm/ps)$
$c^2\ (nm^2/ps^2)$
(1a)
(1b)
(1c)
(1d)
Atomic
1.2
0
-1.2
0.6
0.9
1.8

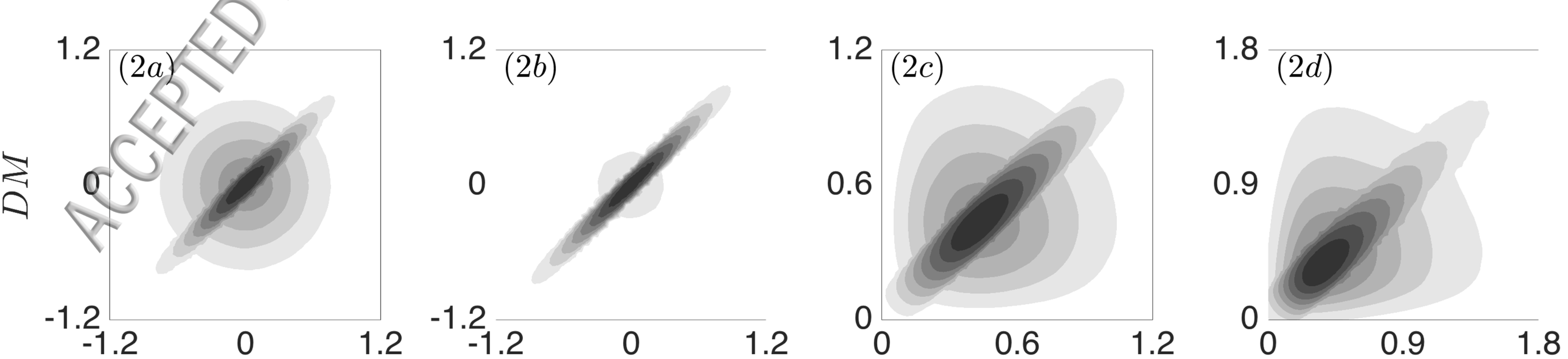

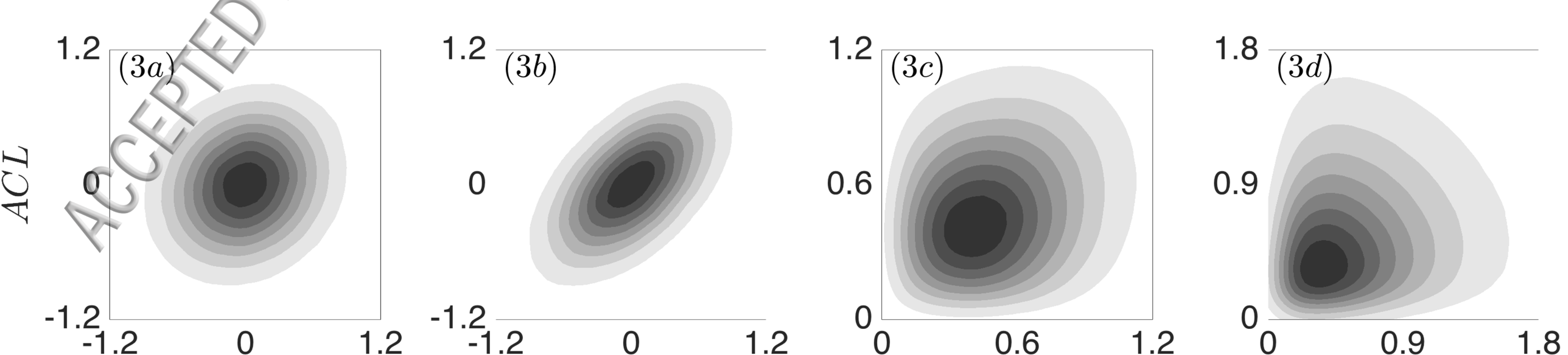
ACL
(3a)
1.2
0
-1.2
-1.2
0
1.2
(3b)
1.2
0
-1.2
-1.2
0
1.2
(3c)
1.2
0.6
0
0
0.6
1.2
(3d)
1.8
0.9
0
0
0.9
1.8

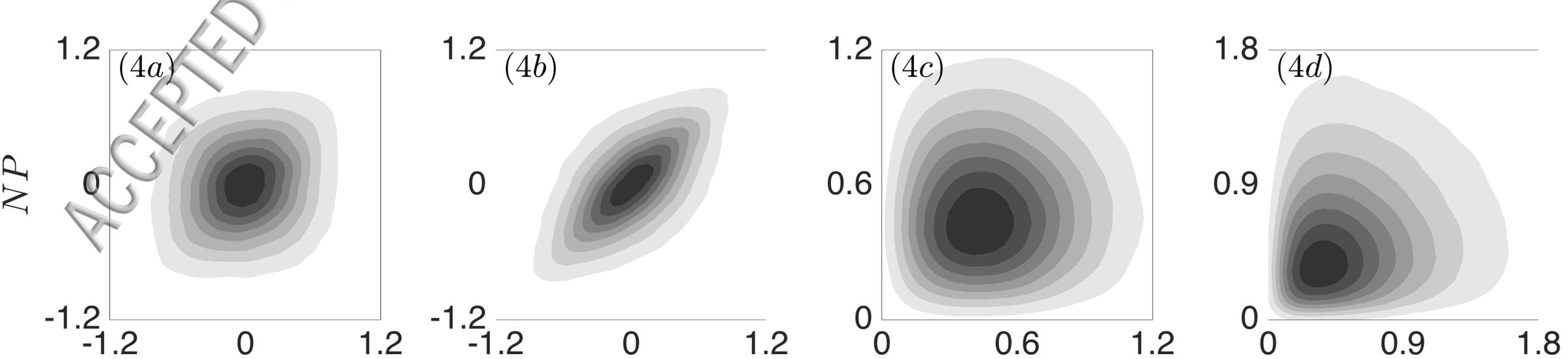

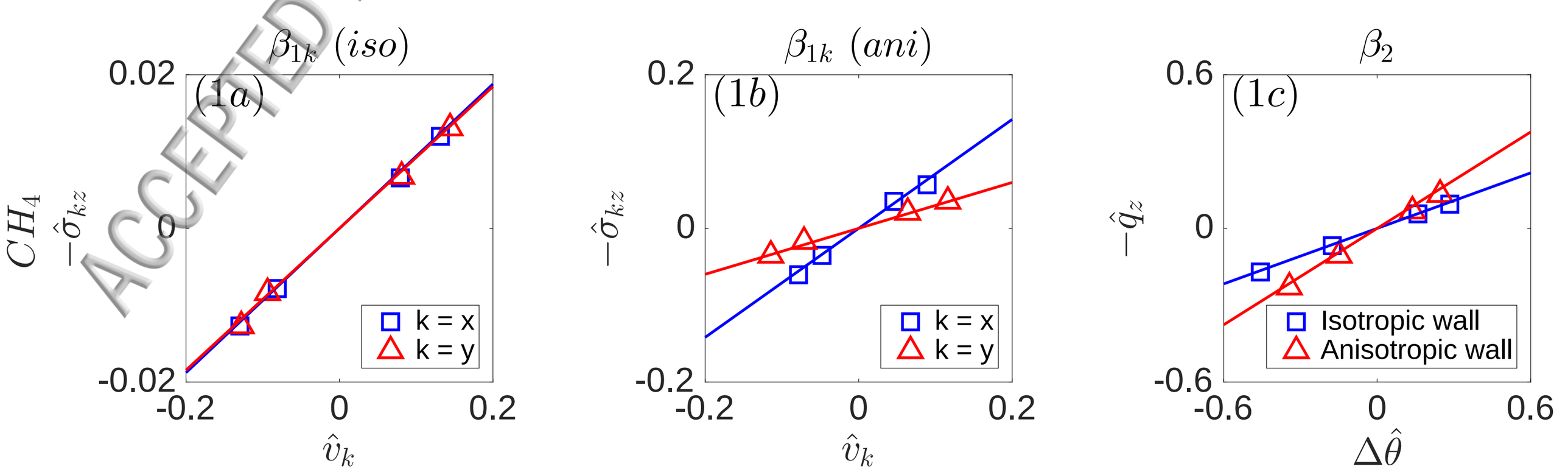
β_{1k} (iso)
(1a)
CH_4
$-\hat{\sigma}_{kz}$
0.02
0
-0.02
-0.2
0
0.2
$\hat{v}_k$
k = x
k = y
β_{1k} (ani)
(1b)
$-\hat{\sigma}_{kz}$
0.2
0
-0.2
-0.2
0
0.2
$\hat{v}_k$
k = x
k = y
β_2
(1c)
$-\hat{q}_z$
0.6
0
-0.6
-0.6
0
0.6
$\Delta\hat{\theta}$
Isotropic wall
Anisotropic wall

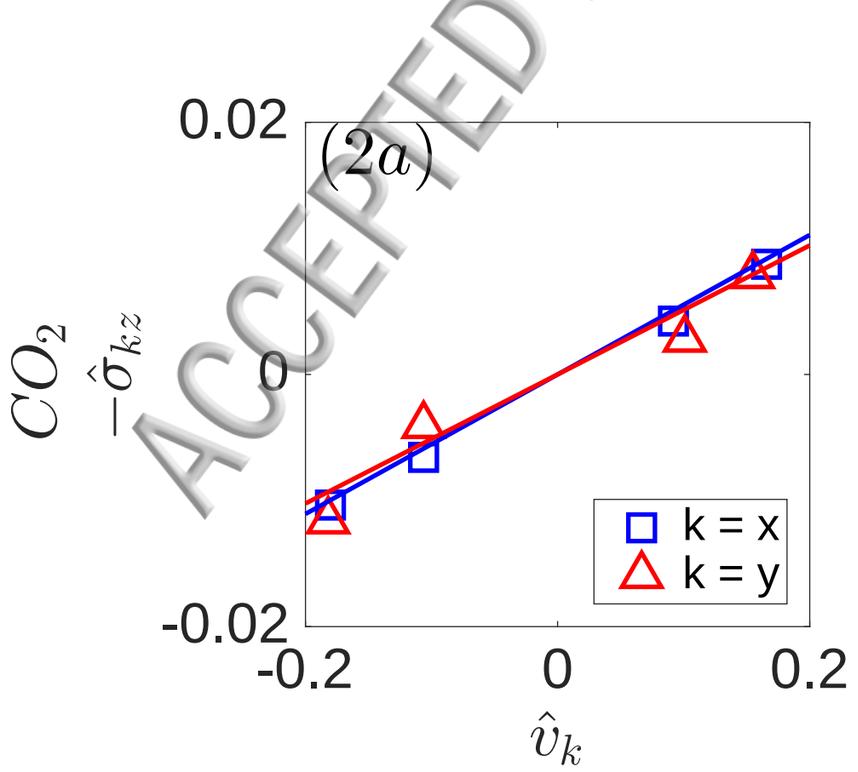
(2a)
CO_2
$-\hat{\sigma}_{kz}$
$\hat{v}_k$
0.02
0
-0.02
-0.2
0
0.2
k = x
k = y

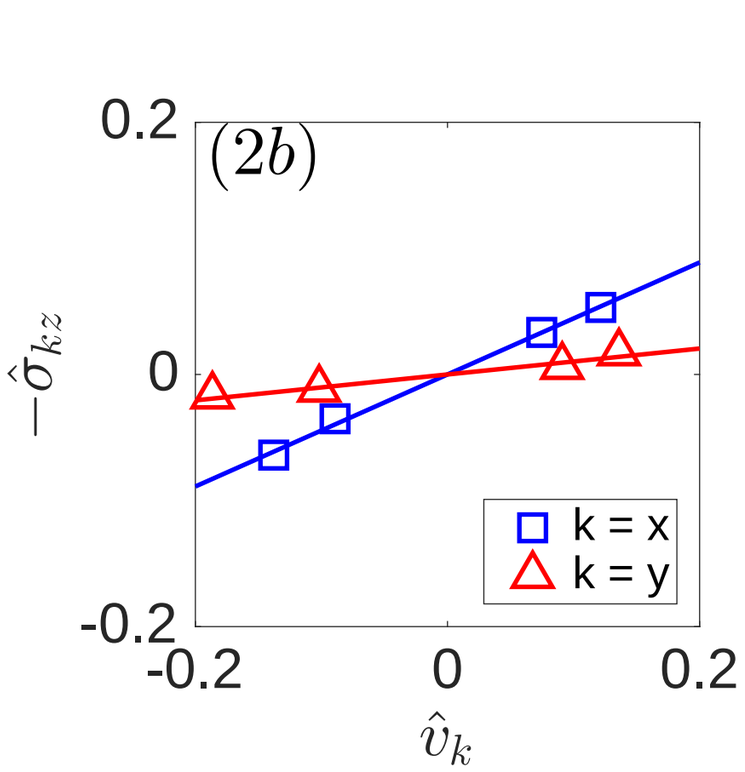
(2b)
$-\hat{\sigma}_{kz}$
$\hat{v}_k$
0.2
0
-0.2
-0.2
0
0.2
k = x
k = y

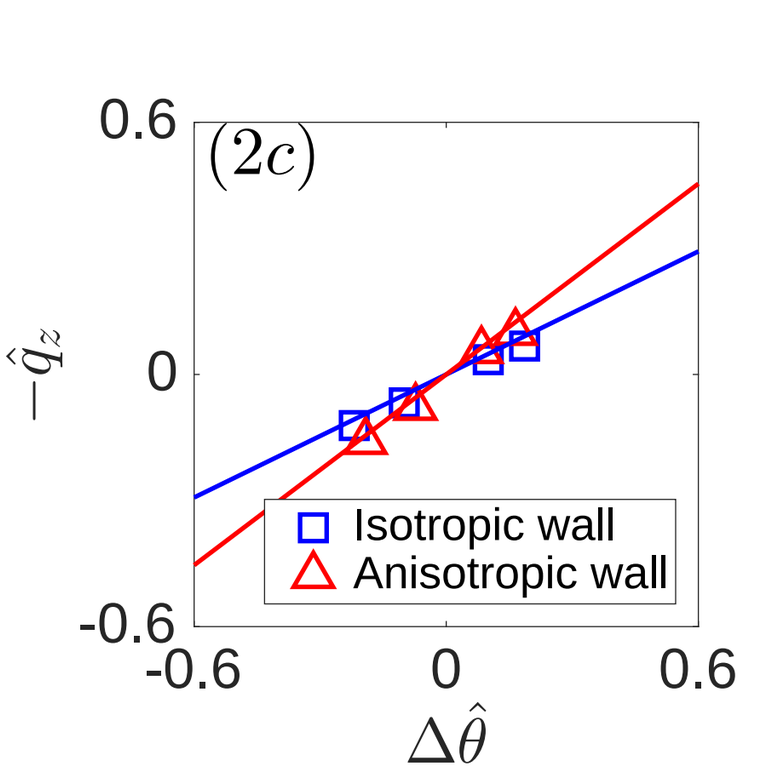
(2c)
$-\hat{q}_z$
$\Delta\hat{\theta}$
0.6
0
-0.6
-0.6
0
0.6
Isotropic wall
Anisotropic wall

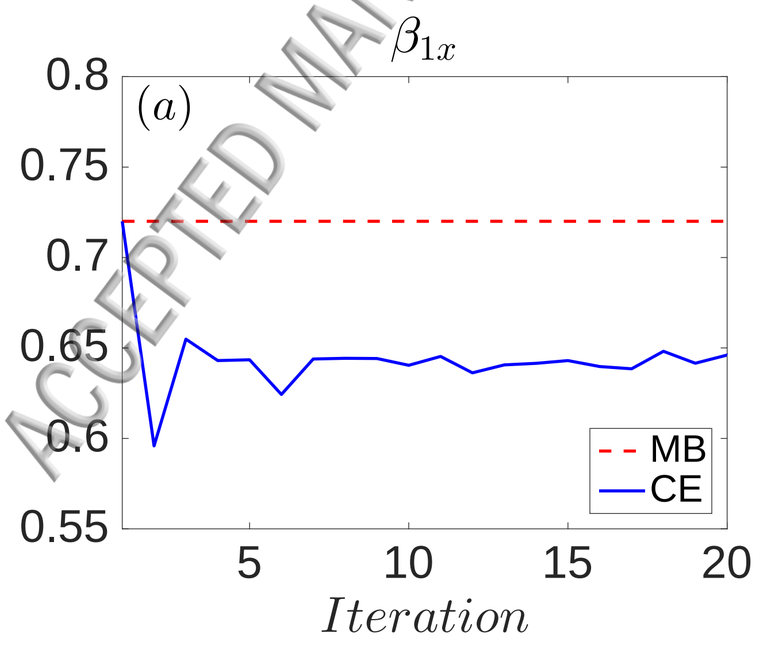

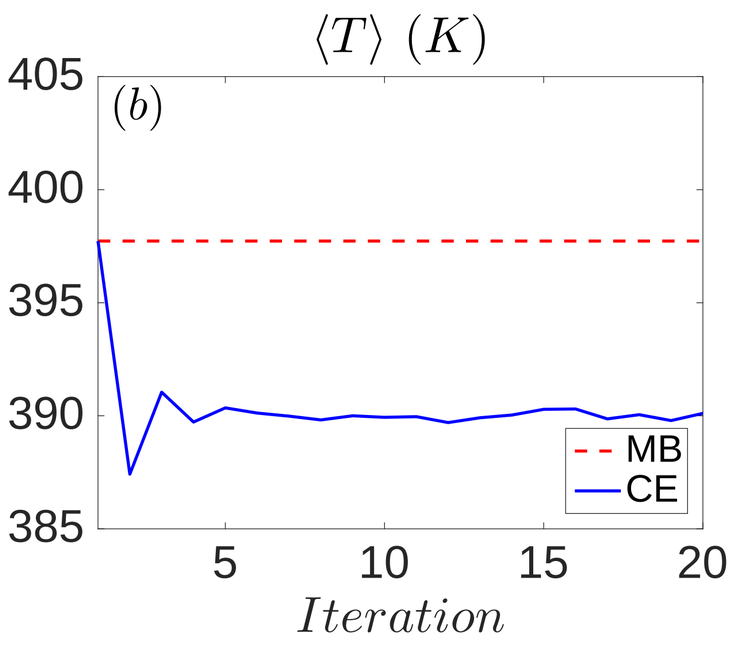

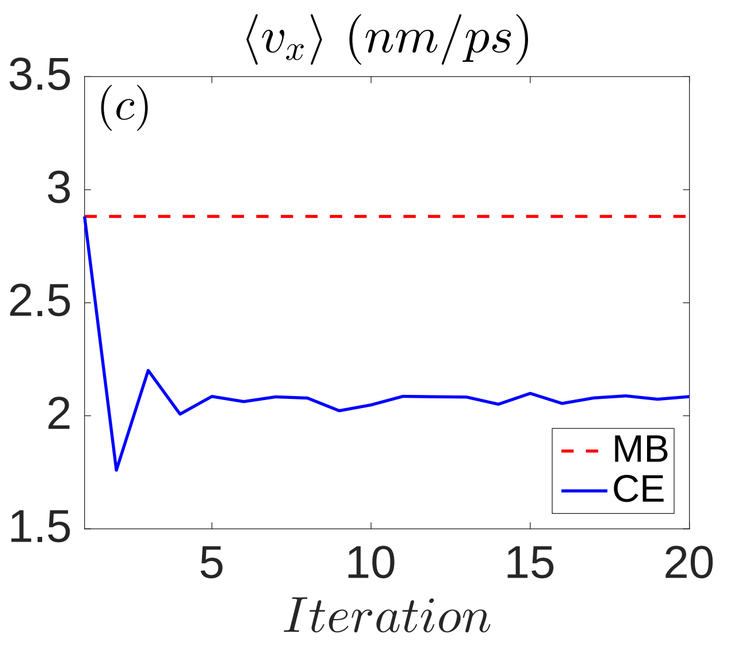

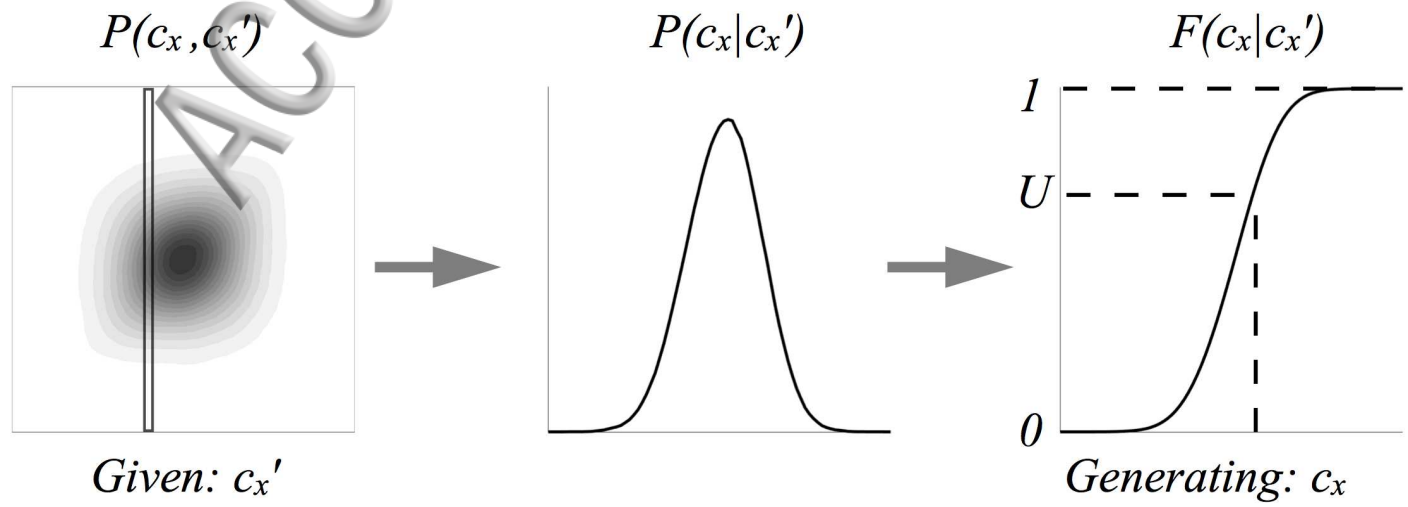
$P(c_x, c_x')$
$P(c_x|c_x')$
$F(c_x|c_x')$
1
U
0
Given: c_x'
Generating: c_x